GIS-based characterization of fault zones in South-Korea using information on seismicity, in-situ stress and slip tendency - Evaluation of respect distances for nuclear waste disposal site screening

Stefan Bredemeyer[1,2,3], Jeoung Seok Yoon[1,4,5], Linmao Xie[1], Jeong-Hwan Lee[6]

[1]Dynafrax UG haftungsbeschränkt, Numerical consulting, Potsdam, Germany
[2]Helmholtz Centre GFZ Potsdam, Section 2.1 Physics of earthquakes and volcanoes, Potsdam, Germany
[3]Geomar Helmholtz Centre for Ocean Research, Kiel, Germany
[4]Helmholtz Centre GFZ Potsdam, Section 2.6 Seismic Hazard and Risk Dynamics, Potsdam, Germany
[5]Handong Global University, Pohang, Korea
[6]Korea Radioactive Waste Agency, Gyeongiu, Korea

Correspondence to: Jeoung Seok Yoon (js.yoon@dynafrax.com); J.H. Lee, (oathway@korad.or.kr)

Abstract. Identification of seismically active fault zones and the definition of sufficiently large respect distances from these faults which enable avoiding the damaged rock zone surrounding the ruptured ground commonly are amongst the first steps to take in the geoscientific evaluation of sites suitable for nuclear waste disposal. In this work we present a GIS-based approach, using the earthquake-epicentre locations from the instrumental earthquake record of South-Korea to identify potentially active fault zones in the country, and compare different strategies for fault zone buffer creation as originally developed for site search in the high seismicity country Japan, and the low-to-moderate seismicity countries Germany and Sweden. In order to characterize the hazard potential of the Korean fault zones, we moreover conducted slip tendency analysis, here for the first time covering the fault zones of the entire Korean Peninsula. For our analyses we used the geo-spatial information from a new version of the Geological map of South-Korea, containing the outlines of 11 rock units, which we simplified to distinguish between 4 different rock types (granites, metamorphic rocks, sedimentary rocks and igneous rocks) and the surface traces of 1,528 fault zones and 6,654 lineaments identified through years of field work and data processing, a rich geo-dataset which we will publish along with this manuscript. Our approach for identification of active fault zones was developed without prior knowledge of already known seismically active fault zones, and as a proof of concept the results later were compared to a map containing already identified active fault zones. The comparison revealed that our approach identified 16 of the 21 known seismically active faults and added 472 previously unknown potentially active faults. The 5 seismically active fault zones which were not identified by our approach are located in the NE- and SW-sectors of the Korean Peninsula, which haven't seen much recent seismic activity, and thus are not sufficiently well covered by the seismic record. The strike directions of fault zones identified as active are in good agreement with the orientation of the current stress field of the peninsula and slip tendency analysis provided first insights into subsurface geometry such as the dip angles of both active and inactive fault zones. The results of our work are of major importance for the early-stage seismic hazard assessment that has to be conducted in support

of the nuclear waste disposal siting in South-Korea. Moreover, the GIS-based methods for identification of active fault zones
and buffering of respect areas around fault zone traces presented here, are applicable also elsewhere.

35

Key words: active fault zones, classification, seismicity, slip tendency, respect distances, South-Korea

1 Introduction

The planning of site investigations for nuclear waste disposal and the spatial assessment of the onsite geological conditions is
40 commonly done by means of Geographic Information Systems, commonly abbreviated as GIS (e.g. Mays et al, 2012; Silva et
al., 2015; Bilgilioglu 2022). Such systems enable compiling extensively large databases containing all spatial information
required to assess the suitability of a site, such as e.g. performing seismic hazard analysis (Lee & Oh, 2022; Sun & Kim, 2017),
and at the same time provide a means to document the progress of site search (e.g. Cheon et al., 2022). For this purpose, the
Korea Institute of Geoscience and Mineral resources KIGAM develops a web-GIS called 'Geo-environmental Information
45 Verification System' (GIVES), which will be made accessible to the public through their website providing an overview of
the individual thematic maps required for site search (KIGAM, 2019).

Large magnitude earthquakes that are capable of rupturing the ground in a deep geological repository are amongst the most
hazardous natural events endangering the confinement of toxic high-level waste, thus it is of major importance to rule out the
presence of seismically active faults in the vicinity of the disposal site (IAEA 2012). This is because active fault zones, i.e.
50 fault zones that are capable to suddenly slip or experience creep during the interseismic period are more prone to rupture again
from static and dynamic stresses they experience, than inactive faults in mechanically more stable crustal blocks (e.g. Rybicki
et al., 1985; Muir Wood & Mallard 1992). It has to be noted though, that intra-continental earthquakes typically occur through
reactivation of previously inactive faults, which particularly applies to faults in collision belts such as found on the Korean
Peninsula (e.g. Kwon et al., 2009; de Jong et al., 2015). Such inactive faults readily can be reactivated by stress redistribution
55 due to change in direction of the crustal movement, the injection of fluids, or by triggering through distant earthquakes or
movements along connected fault systems (e.g. Sibson, 1985; Cappa & Rutqvist, 2011).

The distribution of faults in general, the distribution of active faults, fault scales and respect distances are to be evaluated
during the first stage of the South-Korean site investigations (Choi et al., 2016; Jin et al., 2021). This e.g. can be done by
elaborate field work, or by using different remote sensing techniques such as high-resolution LiDAR imaging or
60 Interferometric Synthetic Aperture Radar (InSAR) capturing the ground surface prior to and after an earthquake (e.g. Ha et al.,
2022; Yun et al., 2019), techniques which are hampered in densely vegetated areas, or by means of seismological studies
linking seismicity to fault zones (e.g. Han et al., 2017).

The objective of the work presented here, was to develop a simple but scientifically sound GIS-based method that utilizes
commonly available data to identify potentially active fault zones in order to assist the planning of future field surveys for the

65 purpose of finding a suitable site for the disposal of high-level radioactive waste (HLW) in South-Korea, or elsewhere. A high probability of activity can be inferred for a fault zone, e.g., if 1) the fault zone overlies a currently seismically active zone and if 2) the fault orientation corresponds to the orientation of the recent regional stress field (e.g. SGD 2020).

Following this rationale, and since the historical and modern instrumental earthquake records in many regions of the world is the only available information on whether a region is seismically active or not, our approach was to use the earthquake-

70 epicentre locations of the earthquake record for the period 1991-01-01 to 2023-05-10 provided by the Korea Meteorological Administration (KMA) to identify potentially active fault zones in South-Korea, according to their location within areas showing high earthquake-density.

For this purpose, we generated heatmaps of the earthquake-epicentre locations in Q-GIS using kernel density estimation, a method suited to identify hot and cold spots in geospatial datasets (e.g. Sun & Kim 2017). This enabled us to determine the

75 spatial earthquake-density of the earthquake catalogue throughout the Korean Peninsula, and to localise earthquake clusters relevant for collocated fault zones. The outlines of earthquake-clusters were then used to determine fault zones touching or intersecting earthquake-clusters and classify them as potentially active. Further, we identified fault zones located within 1 km range of earthquake epicentres to add fault zones which have experienced recent seismic events, but are not located in above mentioned earthquake clusters. The classification results were then compared to a map provided by the National Emergency

80 Management Agency (NEMA 2012) containing those faults which already have been identified as active in the past decades through elaborate field work (Kim et al., 2020).

For further validation of our fault zone classification results and in order to characterise the slip potential of the fault zones in South Korea and their potential to be seismically active, or become reactivated, we moreover performed slip tendency analysis of the determined fault zones according to the approach presented by Röckel et al. (2022). The slip tendency analysis not only

85 provides a quantitative way of mapping fault slip potential, which could be employed as a reference for site search, but also investigates the general influence of the fault geometry, particularly the dip of the fault plane, on the slip potential.

Another task of this work was to define reasonably wide respect zones around the distinguished classes of fault zones in order to exclude the rock volumes which are likely damaged or to be damaged by seismic activity. Here, we discuss different strategies of fault zone length classification and definition of corresponding buffer zones based on fault zone scaling laws (e.g.

90 Wells & Coppersmith, 1984; Barnett et al., 1987; Torabi & Berg, 2011; Torabi et al., 2019), as e.g., were developed for site search by the Nuclear Waste Management Organization of Japan (NUMO 2017), the Federal Company for Radioactive Waste Disposal in Germany (Bundesgesellschaft für Endlagerung; BGE 2022), and the Swedish Nuclear Fuel and Waste Management Company (Svensk Kärnbränslehantering; SKB 2004), and how these could be adopted for the exclusion of unfavourable areas to avoid the damaged rock zone around active fault zones also in South-Korea. For this purpose we compare the results of

95 applying these different fault length classification and buffering methods utilised by Japan, Germany and Sweden to the South-Korean dataset, and show the different areal effects of the so defined exclusion zones on the different host rock types distinguished in this work.

2 Study area

The study focuses on the Geology of the mainland of South-Korea, which has an onshore area of about 100,413 km^2 (as of

100   2020), of which about 99,431 km^2 are available for geoscientific work and chosen for the initial national screening effort of

South-Korea's site search (Figure 1). The Korean peninsula is located on the far eastern margin of the Eurasian plate and has

low to moderate seismicity (Houng & Hong, 2013) in comparison to the surrounding high seismicity regions which are located

more closely to plate boundaries and that are frequently shaken by large magnitude earthquakes (Sun & Kim, 2017). The

geological map presented in Figure 1 below is a result of previous efforts to harmonise existing geological maps of different

105   regions in the country (Cheon et al., 2022). The spatial analyses carried out based on this data aims at supporting the

identification of areas and particularly fault zones in which future geological investigations are to be conducted in more detail

in the field. South-Korea plans to start their site search with a blank white map, and choses to investigate crystalline and

sedimentary rock types as host rock for the deep geological repository (e.g. Kim et al., 2000), as is done in other countries,
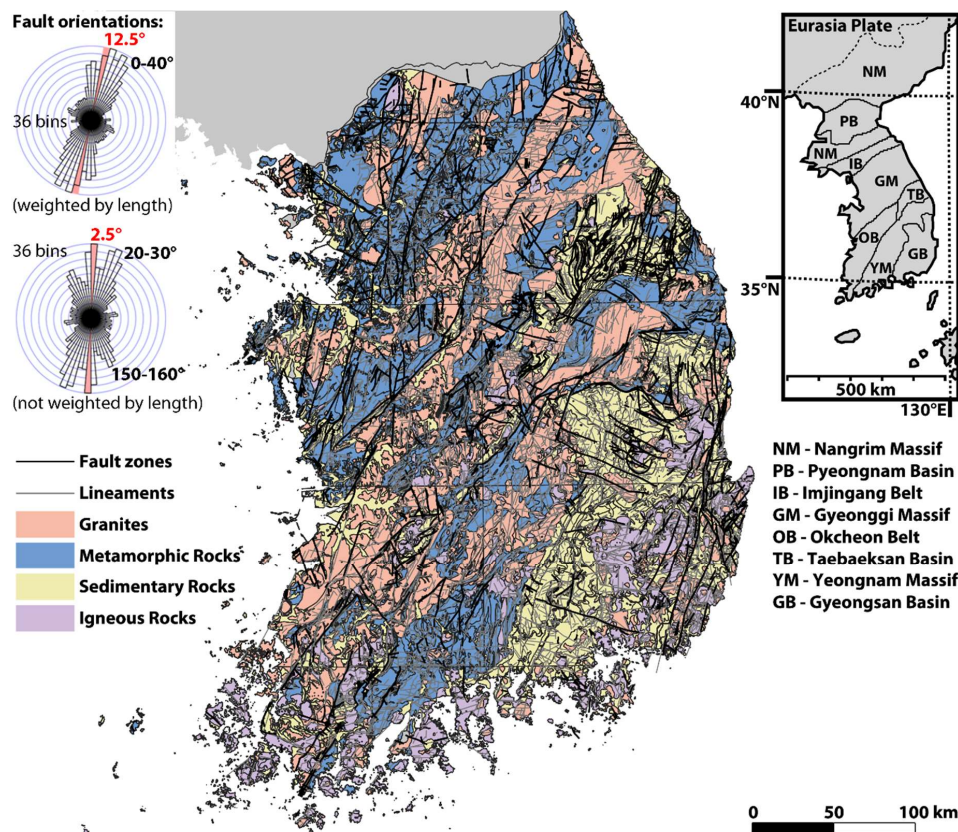
e.g. Germany and Switzerland.

110

Figure 1: Simplified geological map showing the four main rock types distinguished for site search in South-Korea. Rock types distinguished are: 1) orange – granites, 2) blue – deformed/metamorphic rocks (incl. schists and gneisses), 3) yellow – sedimentary rocks and 4) pink – igneous rocks (incl. tuff). Besides 9,204 updated rock unit polygons, the map contains 1,528 surface traces of

115 **currently known fault zones (black lines) and 6,654 other lineaments, respectively morphological edges (grey lines). Sedimentary rock host 45 % of the fault segments, and metamorphic rocks 28 %. Clearly smaller fractions of faults are found in granite (19 %) and igneous rock (7 %) areas. Inset map shows surface traces of major crustal blocks in Korea (modified after Park et al. 2007). Names of crustal blocks separated by major fault systems are indicated below the inset map. Direction histograms at the top left display the preferred orientations of fault zones (top: weighted by length, bottom: not weighted). Mean directions of fault zone trends**

120 **(12.5° if weighted and 2.5° if not weighted by length) are indicated in red. Main directions of major fault zones (if weighted by length) cluster between 0° and 40°, while shorter faults display an additional maximum between 150-160°. (The files required to reproduce this map are the following: Polygons: Data_20230512 — RockTypes.shp, Data_20230512 — ROCk (byRockTY_aggregated)_Collected.shp, Line segments: Data_20230512 — Fault (n=1528).shp, Data_20230512 — Lineament (n=6654).shp, see Table A11 for dataset descriptions)**

125 The potential host rocks available in South-Korea for the construction of a deep geological repository for high-level radioactive

waste storage comprise granites, sedimentary rocks, and metamorphic rocks (Kim et al., 2000), which in total cover about 87

% of the South-Korean mainland (each 29 %), whereas the predominantly less suited igneous rocks merely cover 13 % of the

peninsula (more detailed areal statistics are presented in **Table 1**). Note, that due to the vast occurrence of large Mesozoic granitic plutons covering 29 % of the countries area, here we decided to include gneisses and even the granitic gneisses in the

130 class of *"deformed/metamorphic rocks"* instead of combining it into a *"crystalline rocks"* class together with undeformed granites (and other plutonic rocks) as is done in site selection procedures of other countries, e.g., Switzerland (BFE 2008), Germany (BGE 2020), Sweden (SKB 2011), and Finland (Posiva 2000). This further was done in order to facilitate the visual distinction of deformed and less deformed terrain in South-Korea, which the authors of this work consider being useful both for this study and for further steps of the site search, e.g., if it comes to the exclusion of strongly deformed and/or still deforming

135 large-scale tectonic provinces in the country. A first concept for the Korean reference disposal system for spent fuel in crystalline host rock at depth of 500 m below ground level was developed by the Korea Atomic Energy Research Institute (KAERI) in the framework of 10-years Research & Development program launched in 1997 (Lee et al., 2007). If consumption of nuclear fuel in Korea proceeds as anticipated, wasted fuel will exceed 100,000 MtU in the year 2100, requiring an area of around 20 km^2 in an intact bedrock-block for the construction of an underground storage (Choi et al., 2011), if the dimensions

140 of the storage tunnels of the above mentioned reference repository system are utilised. The least major fault systems and therefore the likely most stable areas on the Peninsula are found in the Precambrian basement of the Yeongnam Massif and the NE-part of the Gyeonggi-Massif (**Figure 1**). According to the conceptual model of the subsurface of the Peninsula developed by Kwon et al. (2009), most of the major SW-NE trending fault systems, particularly those separating crustal blocks (see inset map in **Figure 1**), are dipping towards NW.

145 **Table 1a. Areal statistics of the 4 main rock types distinguished in the simplified geological map of South-Korea. Granites, metamorphic/deformed rocks, and sedimentary rocks each cover about 29 % of the peninsula, whereas igneous rocks merely cover 13 %. Rock types in the table are colour coded according to the legend of the map above (Figure 1). The RGB and HEX-codes of colors used to distinguish different rock types are indicated.**

Rock Types (aggregated)	Map Color	Area km^2	Area %	Perimeter km
Granites	hex(#f7baa6),rgb(247,186,166)	29,095	29	27,458
Deformed Rocks (incl. schist and gneiss)	hex(#6d9bd1),rgb(109,155,209)	28,458	29	40,179
Sedimentary Rocks	hex(#f0ecb0),rgb(240,236,176)	28,891	29	56,117
Igneous Rocks	hex(#cfbada),rgb(207,186,218)	12,987	13	21,666
Sum		**99,431**	**100**	**145,421**

150 **Table 1b. Detailed areal statistics of 11 rock types distinguished in the original non-aggregated version of the geological map of South-Korea. Rock types are colour-coded as above to visualise how the grouping of rock types was done to obtain the aggregated and thus simplified geological map (compare rock types in Table and Figure above). Map colors corresponding to rock type groups defined in Table 1a are indicated in RGB- and HEX-code.**

ROCKTPY_IN	Rock Types (detail)	Map Color	Area km^2	Area %	Perimeter km

편암및편마암	Schist and gneiss	hex(#6d9bd1),rgb(109,155,209)	17,518	17.62	23,032
화강암	Granite		29,095	29.26	27,458
기타 화성암	Other igneous rocks	hex(#cfbada),rgb(207,186,218)	7,078	7.12	12,788
기타 퇴적암	Other sedimentary rocks	hex(#f0ecb0),rgb(240,236,176)	15,814	15.90	20,400
화강암질편마암	Granitic gneiss	hex(#6d9bd1),rgb(109,155,209)	6,994	7.03	8,475
제 4 기 지층	Quarternary strata	hex(#f0ecb0),rgb(240,236,176)	8,917	8.97	23,131
수류지역	Flow area	hex(#f0ecb0),rgb(240,236,176)	1,235	1.24	6,972
석회암	Limestone	hex(#f0ecb0),rgb(240,236,176)	2,324	2.34	4,197
기타 변성암	Other metamorphic rocks	hex(#6d9bd1),rgb(109,155,209)	3,946	3.97	8,672
사암및이암	Sandstone and mudstone	hex(#f0ecb0),rgb(240,236,176)	602	0.61	1,416
응회암	Tuff	hex(#cfbada),rgb(207,186,218)	5,909	5.94	8,879
Sum			**99,431**	**100**	**145,421**

3. Data and methods

155 In this work we focus on the analysis of fault zones of South-Korea with major emphasis of making a first GIS-based pre-survey classification into potentially active and non-active fault zones using the epicentre locations indicated in the South-Korean earthquake catalogue. In order to verify the classification results, and to better characterise fault geometry and slip potential, we moreover conducted slip tendency analyses covering the entire peninsula.

Furthermore, later in the discussion section, we apply different buffering techniques to the South-Korean fault zone dataset,
160 mimicking the methods applied by other countries (Japan, Germany, and Sweden), and compare areas of respect distance polygons surrounding potentially active faults with those of rock unit polygons. The comparison allows first tentative estimates of how much of South-Korea's onshore area likely will not be usable for the disposal of high-level radioactive waste.

The simplicity of our approach is demonstrated by the limited number of datasets required for this type of study, allowing for early application during the course of a site search procedure, possibly also applicable to other places in the world:

165   1. **Fault zone surface traces** (.shp), most recent line segment data provided by KORAD on 2023-05-12
    2. **Earthquake catalogue** (.csv) of instrumental earthquake-record between 1991-01-01 and 2023-05-10 in and around South-Korea, obtained from the National Earthquake Comprehensive Information System (NECIS) operated by the Korea Meteorological Administration (KMA), amongst others containing information on:
        a. Time of occurrence
170   b. epicentre Latitudes, Longitudes (and depths, where available),
        c. earthquake-magnitude scale

3. **Country outline** for masking purposes (.shp), unprojected national (level-0) vector data in decimal degrees provided by GADM (Global Administrative Areas) https://gadm.org/download_country.html (gadm40_KOR_0.shp, gadm40_PRK_0.shp)

175 4. **Rock unit polygons** (.shp), most recent polygons provided by KORAD on 2023-05-12

The workflow used for fault zone classification including the individual steps of the 1) earthquake-cluster analysis, 2) extraction of potentially active fault zones, and 3) slip tendency analysis is illustrated in the flowchart below (**Figure 2**).
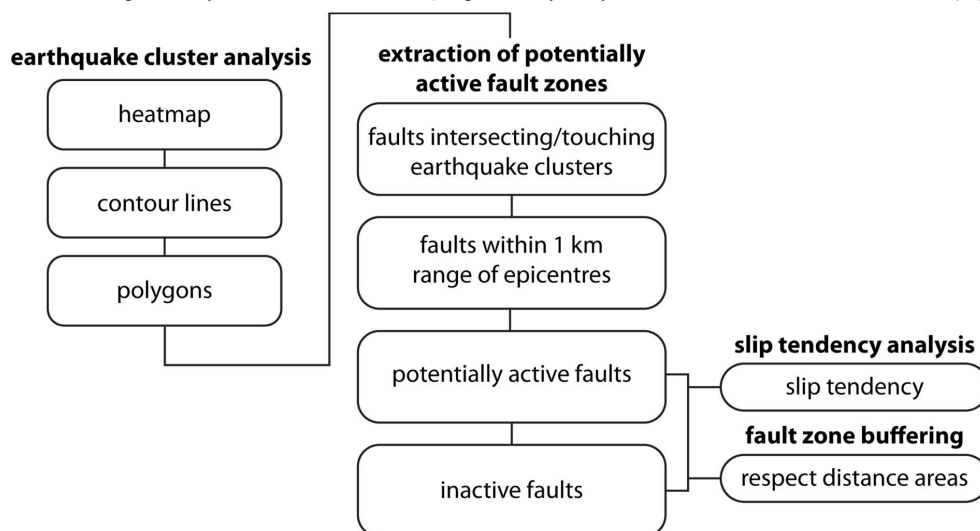
Figure 2. Flowchart illustrating the products of the work steps we applied in our 1) earthquake cluster analysis, 2) extraction of
180 **potentially active fault zones, 3) the slip tendency analysis and 4) fault zone buffering. Individual steps are as follows: 1.1) heatmap production, 1.2) creation of contours around earthquake clusters, 1.3) polygonization of contours around clusters, 2.1) extraction by location of faults intersecting/touching earthquake clusters, 2.2) extraction by location of faults within 1 km range of epicentres. 2.3) merging results of 2.1 and 2.2 to obtain our potentially active faults, 2.4) removal of active faults from the original fault dataset to obtain our currently likely inactive faults data, 3.1) application of slip tendency analyses on both, to the active and the inactive fault**
185 **datasets separately. 4.1) creation of buffers around active and inactive fault zones**

In the following sections we will first give detailed descriptions of the datasets involved in our analysis and the workflow used to yield the outlines of earthquake clusters and the potentially active and inactive fault zone datasets. The results of this classification approach are then discussed in the discussion section along with the results of the slip tendency analysis and the fault zone buffering approaches tested in this work.

190 **3.1 Line segments used for classification: Fault zone surface traces**

The fault zone dataset of South-Korea (Data_20230512 — Fault (n=1528)_ed.shp) currently comprises 1,528 identified fault zone surface traces, which are to be classified (black lines in **Figure 1**). The surface traces of the 1,528 identified fault zones consist of 40,134 georeferenced vertices, and are between 0.16 km and 126 km long (at average 7.81 km, standard deviation

is 10.30 km, median is 4.42 km), and sum up to a total length of 11,941.059 km (Coefficient of Variation: 1.3189, First quartile:
195 2.75 km, Third quartile: 8.85 km, Interquartile Range (IQR): 6.099 km). Distinguished by length according to the fault zone
classification used by KORAD and as given e.g. in Choi et al. (2013), the fault dataset consists of 322 regional fractures (>10
km), 1,131 major local fractures (1-10 km), and 75 minor local fractures (100 m-1 km). The fault length distribution further
shows a pronounced maximum in the 2 – 4 km fault length range, which comprises 485 of the major local fault zones, i.e.
almost a third of the faults in the dataset are in this range, where 277 of the line segments in the fault dataset are between 2
200 and 3 km long, and 208 are between 3 and 4 km long (**Appendix Figure A1**).

Further, the dataset contains 6,654 lineaments (Data_20230512 — Lineament (n=6654)_ed.shp), i.e. linear structures on
Earth's surface, respectively morphological edges, some of which may represent fault surface traces that haven't been
identified as fault zones, yet (grey lines in **Figure 1**). Similarly, as the fault zone dataset, the Lineament dataset moreover is
divided into four categories comprising lineaments of different length: 30 category 4 lineaments shorter than 1 km, 4,019
205 category 3 lineaments of 1-5 km length, 2,357 category 2 lineaments of 5-20 km length, and 248 category 1 lineaments, which
are between 20-170 km long.

In order to determine the spatial coverage of each of the above distinguished four rock types by fault zones and lineaments we
intersected the line traces in the fault- and respectively the lineament datasets with the polygons of the rock type dataset. As a
result, we obtained a fault and a lineament dataset containing information on the lithology corresponding line features intersect
210 (see **Figure 3**).

9
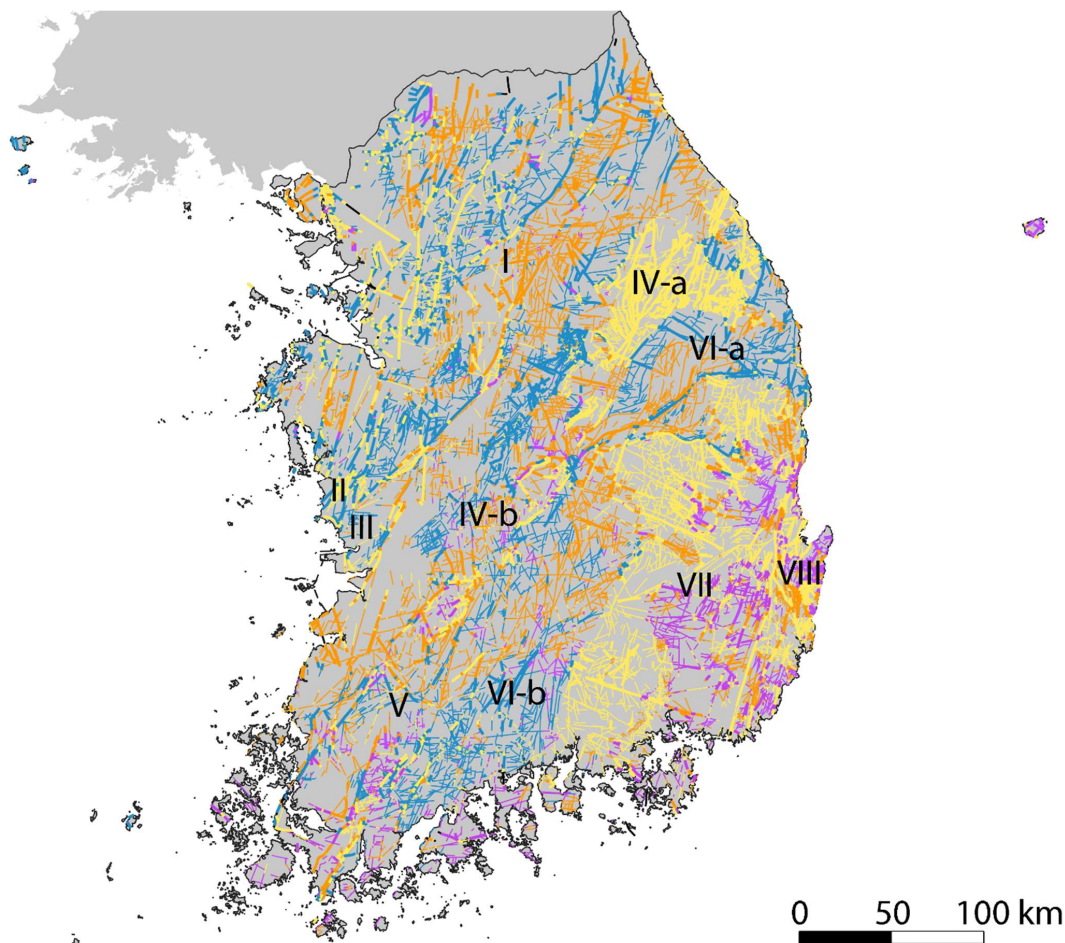
Fault zones, Lineaments	Intersected Rock types	# of faults	% of faults	# of lineaments	% of lineaments
	Granites	551	19	3,086	30
	Deformed Rocks (incl. schist and	948	28	3,370	27
	Sedimentary Rocks	1,510	45	4,362	31
	Igneous Rocks	324	7	1,653	11

Figure 3. Fault zones (thick lines) and lineaments (thin lines) of South-Korea coloured according to the rock type which they intersect. Further, indicated by roman numbers I-VIII are the locations of the eight large scale tectonic provinces in South-Korea (e.g. Kim et al., 2000). The outlines of provinces may be inferred from prominent colour differences between neighbouring faults and lineaments in the map (also compare with Figure 5.18 on p.111 in Kim et al., 2000). The names of the large-scale tectonic provinces, are: I, Gyeonggi massif. II. Chungnam trough. III. Kongju trough. IV. Ogchon belt (a, Nonmetamorphic belt, b,

metamorphic belt), V. Yeongdong-Kwangju trough, VI. Ryeongnam massif (a, Sobaegsan block, b, Jirisan block), VII. Kyeongsang basin, VIII. Yeonil basin. Numbers and percentages of fault surface traces and lineament segments in each of the four rock types are indicated in the legend. Corresponding line segment files are the following: Data_20230512-fault_intersectwith_Rock(byRockTY_aggregated)_Collected_fgeo.shp; Data_20230512-lineament_intersectwith_Rock(byRockTY_aggregated)_Collected_fgeo.shp, see Table A11)

Sedimentary rocks demonstrably are the most fractured rock type, containing 45 % of the fault zone segments and 31 % of the lineament segments, followed by the metamorphic/deformed rocks, which host 28 % and 27 % of the fault zone and the lineament segments, respectively (also compare **Table 2**). Granites still host a significant number of 19 % of the fault segments and 30 % of the lineament segments, while igneous rocks merely contain 7 % and 11 % of the fault and lineament segments, respectively.

The intersection of the fault and the rock type datasets split the originally 1,528 fault surface traces into 3,333 segments which are bound by the rock type polygons of the geological map (detailed statistics in **Table 2**). However, only 38,217 (i.e., 95 %) of the 40,134 fault zone vertices in the dataset were considered as a consequence of that 5 % of the fault vertices are located outside the boundaries of the here considered geological map, that is, a few faults and lineaments are situated offshore, and some faults are located in a buffer zone along the northern border of the country not covered by information on lithology. Intersection of the originally 6,654 lineaments and the polygons of the rock type datasets resulted in 12,471 lineament segments assigned to rock types (details in **Table 3**). As a result of colourizing the faults and lineaments according to the lithology which they crosscut, even the boundaries of the eight large-scale tectonic provinces can be inferred from the map displayed in **Figure 3**. The map in **Figure 3** further reveals large grey areas in which neither faults nor lineaments are mapped. It has to be determined in which places this is due to the lack of information on the occurrence of fractures and in which this is due to actual lack of fracturing. Large unfractured rock volumes are required for the siting of a deep geological repository.

According to Wells and Coppersmiths (1994) empirically determined relationship between Moment Magnitude M and surface rupture length SRL of a fault (M = 5.08 + 1.16*log (SRL [km])), the fault zones investigated in this work, would be capable of producing earthquakes in the magnitude range 4.2-7.5 (**Appendix Figure A2**). Modern canisters for disposal of spent nuclear fuel as e.g. used in Finland and Sweden, and as planned to be used also in Korea (Choi et al., 2013) consist of a copper-shell and a massive cast iron inset, which are designed to withstand an arbitrary shear of 0.05 m (SKB, 2010). Thus, the maximum displacement on a fault cutting through the disposal site shall not exceed 0.1 m according to the results of the safety assessments performed by SKB (SKB, 2010). Relating maximum displacement D_{max} to the surface rupture lengths SRL of the faults in our dataset utilising the regression line (log(D_{max} [m]) = -1.38 + 1.02*log(SRL [km])) of Wells and Coppersmiths (1994), all of the faults considered here would be capable to produce a maximum displacement which exceeds 0.1 m.

Table 2. Faults per Rock type distinguishing 4 rock types. Fault statistics distinguishing 11 rock types are shown in Appendix Table A1. Total area sizes of rock types are compared to sum of lengths of all fault segments in each rock type, # of fault segments per rock type, % of faults per rock type, average fault segment lengths per rock type. Further, the earthquake magnitudes the faults in each rock type are capable of according to the surface rupture length to moment magnitude relationship were determined by Wells and Coppersmith (1994). (Corresponding line segment file produced for this work is the following: Data_20230512-fault_intersectwith_Rock(byRockTY_aggregated)_Collected_fgeo.shp, see Table A11)

Rock types (aggregated)	Area km²	Area %	Sum of fault segment Length km	# of fault segments	% of fault segments	Average fault segment Length	Average EQ-Magnitude (WC94)
	km²	%	km	#	%	km	M
Granites	29,095	29	2,255	551	19	4.09	6.04
Deformed Rocks (incl. schist and gneiss)	28,458	29	3,335	948	28	3.39	5.95
Sedimentary Rocks	28,891	29	5,314	1,510	45	2.96	6.03
Igneous Rocks	12,987	13	811	324	7	2.49	5.99
Sum	**99,431**	**100**	**11,715**	**3,333**	**100**	**3.23**	**6.01**

Table 3. Lineaments per rock type stats distinguishing 4 rock types. Lineament statistics distinguishing 11 rock types are shown in
255 Appendix Table A2. Total area sizes of rock types are compared to sum of lengths of all lineament segments in each rock type, # of lineament segments per rock type, % of lineaments per rock type, and average lineament segment lengths in each rock type are indicated. (Produced line segment file: Data_20230512-lineament_intersectwith_Rock(byRockTY_aggregated)_Collected_fgeo.shp, see Table A11)

Rock Types (aggregated)	Area km²	Area %	Sum of lineament segment Length km	# of lineament segments	% of lineament segments	Average lineament segment Length
	km²	%	km	#	%	km
Granites	29,095	29	12,451	3,086	30	4.03
Deformed Rocks (incl. schist and gneiss)	28,458	29	11,190	3,370	27	3.23
Sedimentary Rocks	28,891	29	12,700	4,362	31	2.46
Igneous Rocks	12,987	13	4,561	1,653	11	2.92
Sum	**99,431**	**100**	**40,903**	**12,471**	**100.00**	**3.16**

260 **3.2 Point Cloud used for earthquake-cluster analysis: earthquake-catalogue (epicentre locations)**

The earthquake catalogue we used for our earthquake cluster analysis spans the magnitude 2.0 to 5.8 earthquakes recorded between 1991-01-01 and 2023-05-10 in and around South-Korea (KMA, https://www.weather.go.kr). The catalogue contains information on 1,943 earthquake events with an average magnitude of 2.6 (see **Figure 4**). The coordinates for the relocated events in this catalogue are given at a spatial resolution of 0.01 decimal degrees, i.e. about 1.11 km. Older earthquake
265 compilations, such as that catalogued from Korean historical documents, containing 2,186 historical earthquakes that occurred in Korea in the period between 2 and 1904 A.D. (e.g. Lee & Yang, 2006), and the 323 monitored events of the period 1905 to 1945 (Lee et al., 2003) were not considered here, due to the low accuracy of the locations of merely 0.1 decimal degrees, i.e. about 11.1 km.

12
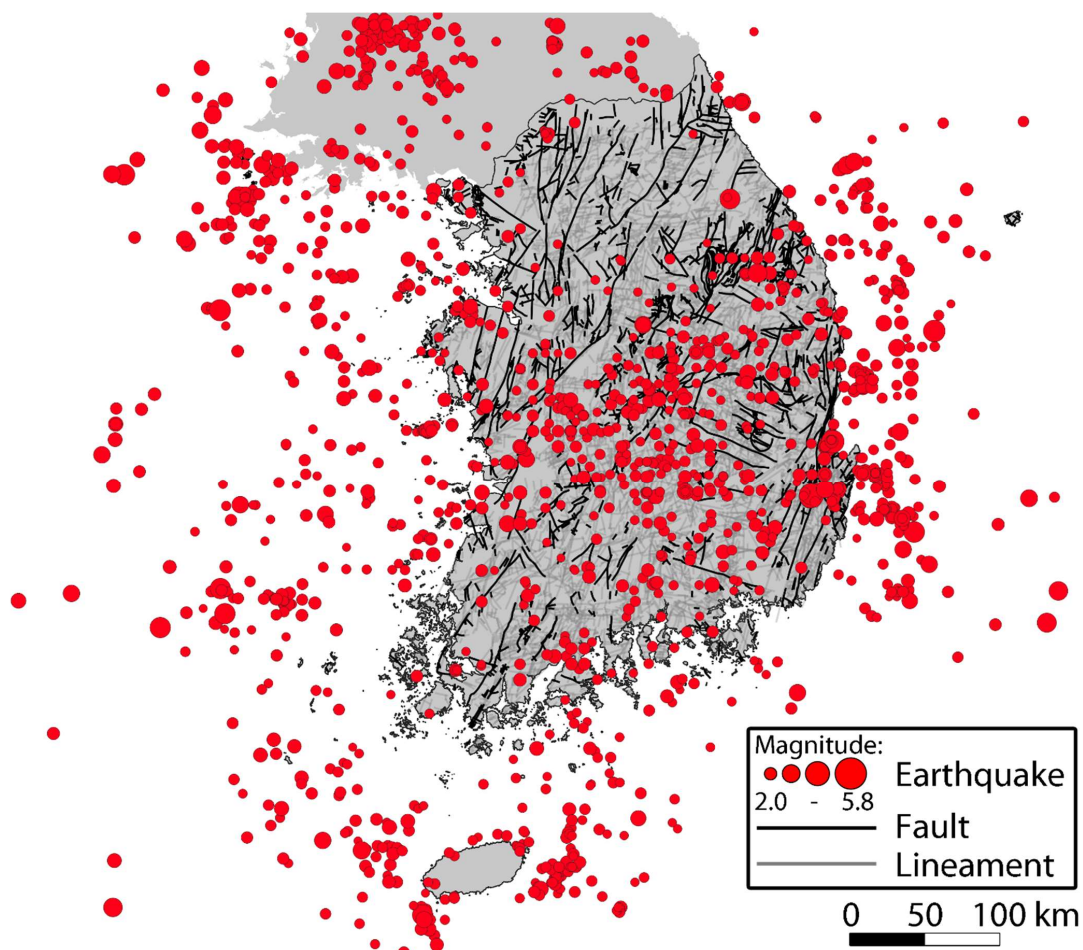
Figure 4. Earthquake epicentres recorded between 1991-01-01 and 2023-05-10 in and around South-Korea. Earthquake epicentre-symbols (red circles) are sized by earthquake magnitude. (Point cloud file shown here is available as: KoreaEQ_1991-01-01_2023-05-10.shp, see Table A11)

Most epicentres of historic M 2.0-5.8 earthquakes which occurred in and around South-Korea in the period 1991-2023 are located in the central highlands of the South-Korean peninsula (**Figure 4**). Further, there are several offshore earthquake clusters, which amongst others are draped around the west coast, form a continuous ridge at about 100 km distance parallel to the east coast and an about 300 km broad batch covering Jeju volcanic island in the South. Notably, there are very large zones in the country which have seen a very low seismic activity in the period covered by the instrumental record. These zones extend almost over the entire Northern third and the Southern third of the country, thus resulting in a tripartite zoning of the

13

spatial earthquake density. Relocated hypocentres of the earthquakes are situated down to a depth of 35 km within the

280   seismogenic crust. 849 of the 1,943 earthquakes occurred onshore in the area considered for site search on the Korean Peninsula. Most of the earthquake epicentres onshore of the Peninsula are located in sedimentary rocks (45 %), 25 % of the earthquakes occurred in granite areas, and about 15 % of the earthquakes happened each in areas consisting of deformed and igneous rocks (**Table 4**).

285   **Table 4. Number of earthquake occurrences in each rock type distinguishing 4 rock types. Statistics of earthquake occurrences distinguishing 11 rock types are shown in Appendix Table A3.**

Rock Types (aggregated)	Area (km^2)	Perimeter (km)	# of epicentres in rock type polygons	% of epicentres in rock type polygons
Granites	29,095	27,458	212	24.97
Deformed Rocks (incl. schist and gneiss)	28,458	40,179	133	15.67
Sedimentary Rocks	28,891	56,117	383	45.11
Igneous Rocks	12,987	21,666	121	14.25
Sum	**99,431**	**145,421**	**849**	**100**

3.3 Earthquake density map creation

Heatmaps are a common way of analysing spatial variations in point cloud data by means of generating a raster image

290   representation which is interpolated over the extent of the point cloud, i.e. transforming point data to areal information.
Here, heatmaps of the earthquake catalogue were generated by means of the Kernel Density Estimation (KDE) algorithm integrated in Q-GIS, in order to analyse the spatial distribution of earthquake clusters on the Korean peninsula. Kernel density estimation is commonly used to estimate the probability density function of a dataset (e.g. Węglarczyk 2018) and widely applied for heat-map production (Yuan et al., 2019).

295   Point cloud cluster analysis using heatmaps usually requires finding a suitable size, respectively bandwidth for the kernel utilised for density estimation. Bandwidth selection always is a compromise between obtaining the highest possible detail for the analysis and capturing the really important features (e.g. Chen, 2017). Small scale features may clutter the view on really important large-scale features and earthquake clusters may extend over larger areas than the smallest reasonable kernel size (corresponding to the best resolution) and thus in some instances may graphically be better presented using larger smoothing

300   kernels for the heatmap generation, than if using smaller ones.
We analysed the spatial epicentre density of the earthquake catalogue over the South-Korean mainland via kernel density estimation and applied different kernel-radii in the range 10 km to 150 km and pixel-sizes of 1 and 0.1 km to the epicentre point cloud, in order to find the most suited combinations of search kernel radius (i.e. the area to be smoothed over in a heatmap), and pixel size (i.e. resolution of resulting raster image) for the two following purposes:

305   1) creation of a heatmap for *illustration of the clustering of earthquake epicentres in space*, and the identification of faults touching or intersecting these potentially active areas, and

2) creation of a heatmap for *identification of fault surface traces within 1 km radius of the epicentres*.

A pixel size of 1 km was chosen for the generation of the two heatmaps, to make best use of the spatial resolution of the earthquake catalogue (0.01 decimal-degree, i.e. about 1.1 km).

310   For heatmap 1) the determination of earthquake clusters, a kernel radius of 10 km was chosen to ascertain sufficient clustering of epicentres, because diameters of typical earthquake clusters in the South-Korean catalogue are about 20 km across. Resulting heatmap is shown in **Figure 5**.

Worksteps for EQ-density map production and extraction of earthquake-cluster outlines

1. Import EQ-epicentre location data into Q-GIS (\Layer\Add Layer\Add Delimited Text Layer „EQcatalog.csv")
315   2. Generate heatmaps of the EQ epicentre distribution using kernel density estimation
   a. Apply KDE to EQ-catalogue data (generates a raster image of EQ-event density from the point cloud, \Processing Toolbox\Interpolation\Heatmap (Kernel Density Estimation))
   b. Extract Contour lines from raster image (\Raster\Extraction\Contour)
   c. Add Geometry Attributes to contour lines (\Vector\Geometry Tools\Add Geometry Attributes)
320   d. Lines to Polygons (\Vector\Geometry Tools)

For heatmap 2) the earthquake-fault collocation analysis the kernel radius was reduced to 1 km, to resolve the locations of epicentres. In this case, using the same value, i.e. 1 km both for the kernel radius and for the pixel size resulted in 2x2 km sized box-shaped search kernels (**see Appendix Figure A3**), rather than applying a steady 1 km circular radius. This slight enlargement of the search kernel area in comparison to a more circular area if using a smaller pixel size of 0.1 km, resulted in

325   picking 163 instead of only 128 earthquake events in the vicinity of known faults in South-Korea.

**Worksteps for colocation of EQ-epicentres and fault zones**

1. Import EQ-epicentre location data into Q-GIS (\Layer\Add Layer\Add Delimited Text Layer „EQcatalog.csv")
2. Generate search kernels of the EQ epicentre distribution using kernel density estimation
   a. Apply KDE to EQ-catalogue data (generates a raster image of localised search kernels from the point
330   cloud, \Processing Toolbox\Interpolation\Heatmap (Kernel Density Estimation))
   b. Polygonize the search kernel cloud (\Raster\Conversion\Polygonize: Raster to vector, GDAL toolbox)
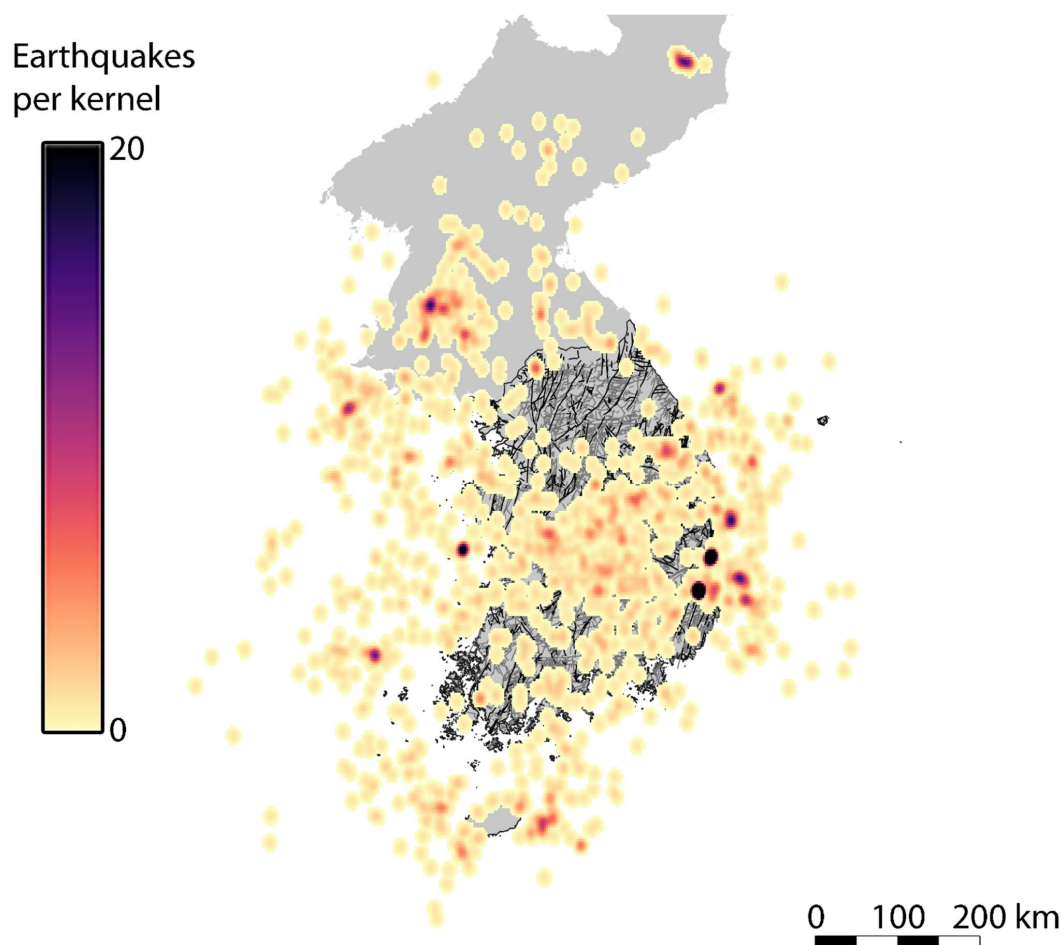
Figure 5. Earthquake-density heatmap obtained by kernel density estimation (KDE) from the instrumental historical earthquake record in and around South-Korea between 1991 and 2023. Kernel radius is 10 km and pixel size is 1 km. (Raster image product shown here: KoreaEQ_HeatmapKDE_Radius0.1degPxSize0.01.tif, see Table A11)

A contour map was then created from this heatmap raster image data (**Figure 6**), in order to enable working with the heatmap information as a tool for selecting defined areas in other datasets such as our fault zone traces located within earthquake clusters. Shown below is the contour line plot derived from the heatmap using a smoothing kernel radius of 10 km.

16
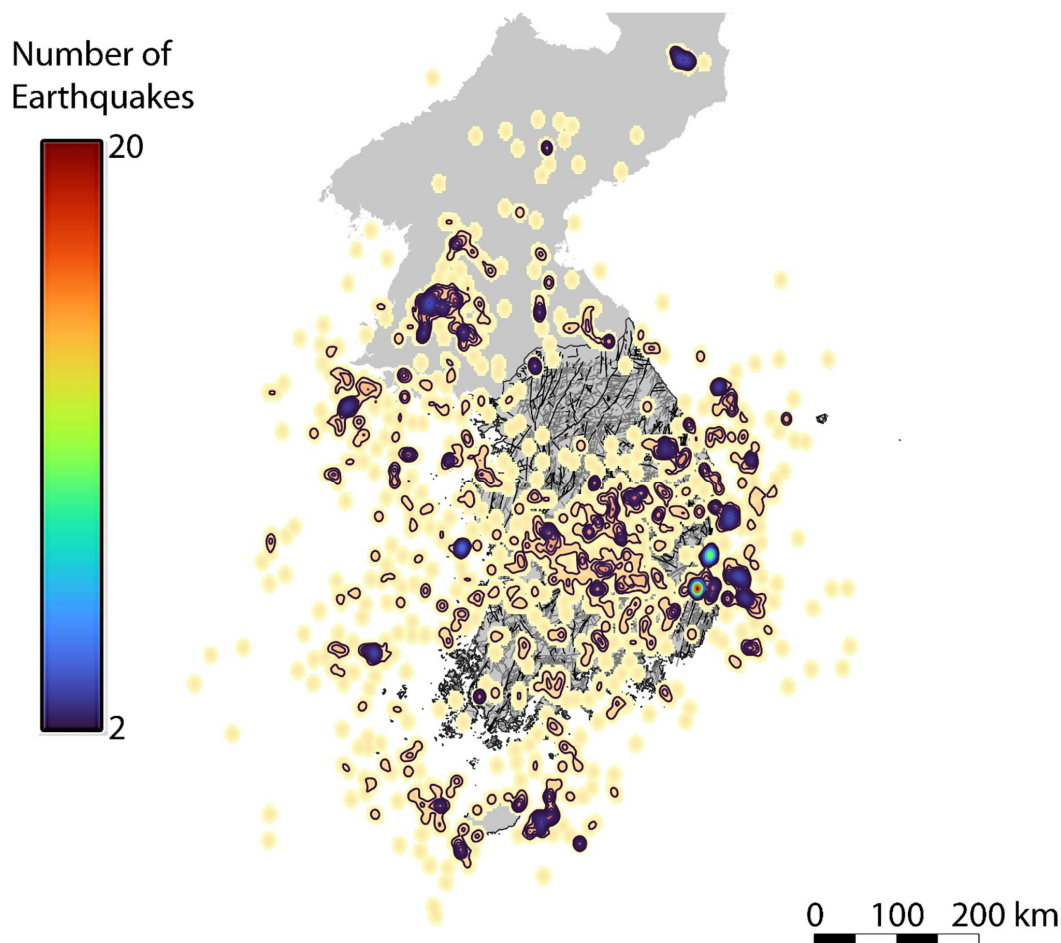
Figure 6. Heatmap of earthquake epicentres as in Figure 6, here showing Earthquake density contours at intervals of 1-200 epicentre locations per smoothing kernel. Level 1 contours indicate the presence of at least two epicentres forming a cluster which were accepted as outlines used for selection of the fault zones to be classified as potentially active and thus to be avoided in the site planning for a deep geological repository. (Contour lines: KoreaEQ_HeatmapKDE_Radius0.1degPxSize0.01_contoursInterval1.shp, see Table A11)

The level 1 contours of the earthquake density heatmap were then transformed to polygons, in order to define the areas used for extraction of touching or intersecting fault zones. The transformation of all above shown level-1 contour lines of the heatmap into polygons yielded 169 earthquake-clusters, 78 of which are located on South-Korean mainland. They cover an area of 48,442.0 km², and the size of individual clusters ranges between 1 km² and 6,235.0 km². On land, the 78 earthquake

17

epicentre clusters cover an area of 20,081 km², that is about one fifth of the South-Korean mainland (100,210 km² as of 2020)
(see **Table 5** and **Appendix Table A4** for areal statistics). (The Polygon files obtained through polygonization of the level 1

355 contours   shown   above   are   the   following: KoreaEQ_HeatmapKDE-
Rad0.1contour_geometry_polygons_geometry_outerbound.shp,   KoreaEQ_HeatmapKDE-
Rad0.1contour_geometry_polygons_geometry_outerbound_mainland.shp, see Table A11)

Calculation of the overlap between the onshore earthquake clusters and the rock type boundaries in the geological map revealed
that the earthquake cluster areas are more or less evenly distributed amongst the rock types (**Table 5**). The largest area covered

360 by these onshore earthquake clusters is hosted by Granites, where these in total cover 6,626 km², which corresponds to about
7 % of the countries area and 33 % of entire granite outcrop area. Second largest area affected by earthquake clusters, covers
6,407 km² in sedimentary terrain, which is 6 % of the country area and 32 % of the sedimentary coverage. The total area of
earthquake clusters in deformed (or metamorphic) rocks is 4,516 km², which corresponds to 5 % of the country and 23 % of
the deformed rock area, respectively. Igneous rocks host a negligible 2,510 km² large area, comprising merely 3 % of the

365 country and 13 % of the total area of the igneous rock type. As would be expected, these numbers compare well to the
observations made for the spatial earthquake distribution in areas of the 4 different rock types, as is described above (compare
Figure 4, and **Table 4**).

Table 5. Rock type area covered by the onshore earthquake clusters obtained from the heatmap map contours shown in Figure 8. distinguishing 4 rock types. Earthquake cluster areas distinguishing 11 rock types are listed in Appendix Table A4.

Rock Types (aggregated)	Area km²	Area %	KDE-Rad0.1 area km²	KDE-Rad0.1 area % of country	KDE-Rad0_1 area % of rock type
	km²	%	km²	%	%
Granites	29,095	29	6,626	7	33
Deformed Rocks (incl. schist and gneiss)	28,458	29	4,516	5	23
Sedimentary Rocks	28,891	29	6,407	6	32
Igneous Rocks	12,987	13	2,510	3	13
Sum	**99,431**	**100**	**20,058**	**20**	**20**

370 The heatmap required for identification of fault surface traces within 1 km radius of the epicentres in contrast merely required
being   polygonised   in   order   to   fulfil   its   purpose   (see   **Appendix   Figure   A3**).   (Raster   image:
KoreaEQ_HeatmapKDE_Radius0.01degPxSize0.01.tif;   Polygons: KoreaEQ_HeatmapKDE_Radius
0.01degPxSize0.01_Polygons_geometry.shp,   KoreaEQ_HeatmapKDE_Radius
0.01degPxSize0.01_Polygons_geometry_mainland.shp, see Table A11)

375 **3.4 Identification, respectively rule-based extraction of potentially active fault zones**

For identification of potentially active faults in South-Korea, we extracted faults by location according to the two following rules:

- **Rule 1)** Extraction of **faults which touch or intersect pre-determined earthquake-epicentre clusters**. Application of this rule resulted in the selection of 457 fault zone segments and was aimed at finding faults that are
380 particularly at risk of being active, even though not necessarily located aside an earthquake epicentre.
- **Rule 2)** Extraction of **faults within 1 km range** (or rather 2 x 2 km square area) **of an earthquake epicentre**. Application of this rule resulted in selection of 163 faults. It was intended to collocate features of the fault database and event locations of the earthquake database which are sufficiently close to confidentially assume a causal relationship and connect them by application of this rule.

385 Comparing the extracted features from rules 1 and 2, there is a large intersection between the two groups, where faults fulfilled both rules 1 AND 2. 128 of the faults found by rule 1, additionally are within 1 km range of an earthquake epicentre and touch or intersect an earthquake cluster. Only 35 of faults picked by rule 2) do not touch or intersect pre-determined earthquake-epicentre clusters at the same time.

4.Results

390 Aim of this work was to identify and extract potentially active faults using information on earthquake epicentre locations from the 1991-2023 earthquake-catalogue of South-Korea as provided by KMA. The feature extraction described in previous section yielded 2 largely overlapping sets of in total 488 fault surface traces, which in the following are to be classified as "potentially active in recent times", and a remainder of 1,040 fault zones which, at least according to the earthquake catalogue, are not located in immediate proximity to regions of recent earthquake activity.

395 457 of the 1,528 known fault zones in South-Korea intersect one or more of the 78 earthquake- clusters which were identified in this study onshore South-Korea using kernel density estimation to assess the spatial earthquake-epicentre distribution of the 1991-2023 earthquake- catalogue of that region. 163 of 1,528 fault zones are located within 1 km range of one or more of the 1991-2023 earthquake-epicentres. 128 of these 163 faults intersect earthquake-clusters and are within 1 km range of an earthquake-epicentre. Only 31 of these 163 faults do not intersect an earthquake-cluster at the same time.

400 That is, 457+31=488 i.e. about one third of the 1,528 known fault zones in South-Korea have to be considered potentially active according to their spatial proximity to locations of recent earthquake-activity (**Figure 7**). Remaining 1,040 faults neither touch or intersect earthquake clusters, nor are they within 1 km range of any earthquake epicentre in the 1991-2023 catalogue, and thus were classified as currently not active.
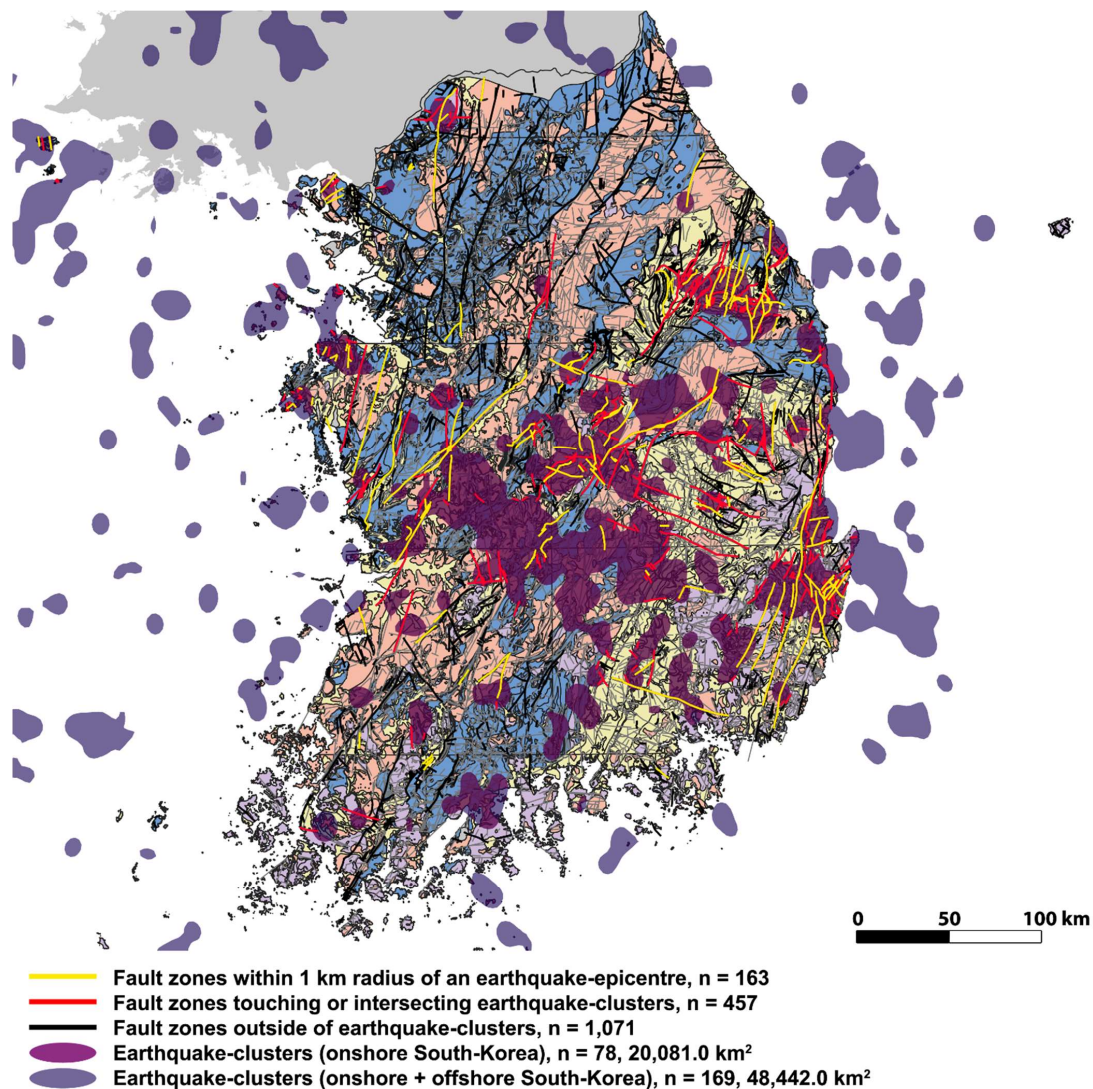
Figure 7. Results of the fault zone classification on top of determined earthquake epicentre clusters onshore and offshore South-Korea and distinguished rock types (granites, deformed rocks, sedimentary rocks and igneous rocks). Fault zones which touch or intersect earthquake clusters are displayed by red lines, fault zones within 1 km radius of an earthquake epicentre are shown as yellow lines. 128 of the yellow lines at the same time belong to the class of faults which touch or intersect earthquake-clusters (displayed by red lines). This large overlap becomes clearer in Appendix Figure A4 where the yellow lines, here displayed on top of the red lines, are displayed in a layer below the red lines, i.e. in vice-versa order.

Comparing the length statistics of the entire fault dataset with those of the two subsets of faults picked as potentially active and the intersection of the two subsets, shows that 6,873 of the in total 11,941 fault length kilometres are to be considered active (**Appendix Table A6 and Figure A5**).

Fault orientations of the two fault zone groups identified as potentially active and the orientations of the fault zones derived from the intersection between the two groups are characterised by two prominent trends, which are narrowed down to a much tighter range of directions if compared to the fault orientations of the entire dataset displayed in **Figure 1**. Rose diagrams of the two subsets of potentially active fault zones containing 457 and 163 fault surface traces, respectively, and their intersection comprising 128 fault surface traces are shown below (**Figure 8**).
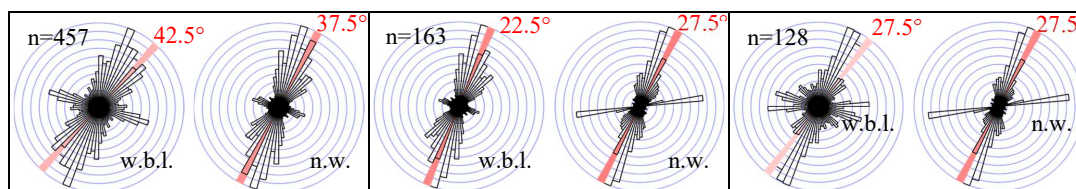

Figure 8. Rose diagrams of the two extracted fault zone groups and their intersection (w.b.l.: weighted by length, and n.w.: not weighted). Left: Potentially active fault zones picked by Rule 1 (457 fault zones touching or intersecting earthquake-clusters). Middle: Potentially active fault zones picked by Rule 2 (163 fault zones within 1 km of earthquake-epicentres, i.e. 2x2 km search kernel). Right: Potentially active fault zones picked by both, Rules 1&2 (128 fault zones intersecting earthquake-clusters and within 1 km of earthquake-epicentres).

Most of the 488 fault zones identified as potentially active show a NNE-SSW trend, clustering between 15° and 40°, with a maximum at about 20°, and a minor subset of the faults display a WNW-ESE trend ranging between about 100° and 110°. Additionally, the rose diagrams of the 163 faults within 1 km range of an earthquake epicentre including the 128 faults which additionally touch an earthquake-cluster (middle and right of **Figure 8**), and particularly the short fault segments in these groups (see diagrams not weighted by length) show a prominent SSW-NNE-trend between 80 and 90°.

For further analysis the two potentially active fault zone groups (yellow and red in Figure 7) were combined into one dataset (**Appendix Figure A6**). Intersection of the line segments in the potentially active fault zone dataset with the rock type polygons shows that slightly more than half of the fault zone segments (53 %) are hosted by sedimentary rock types, while Granites and deformed rocks host about 19 % each, and 8 % are hosted by igneous rocks (**Figure 9, Table 6**).
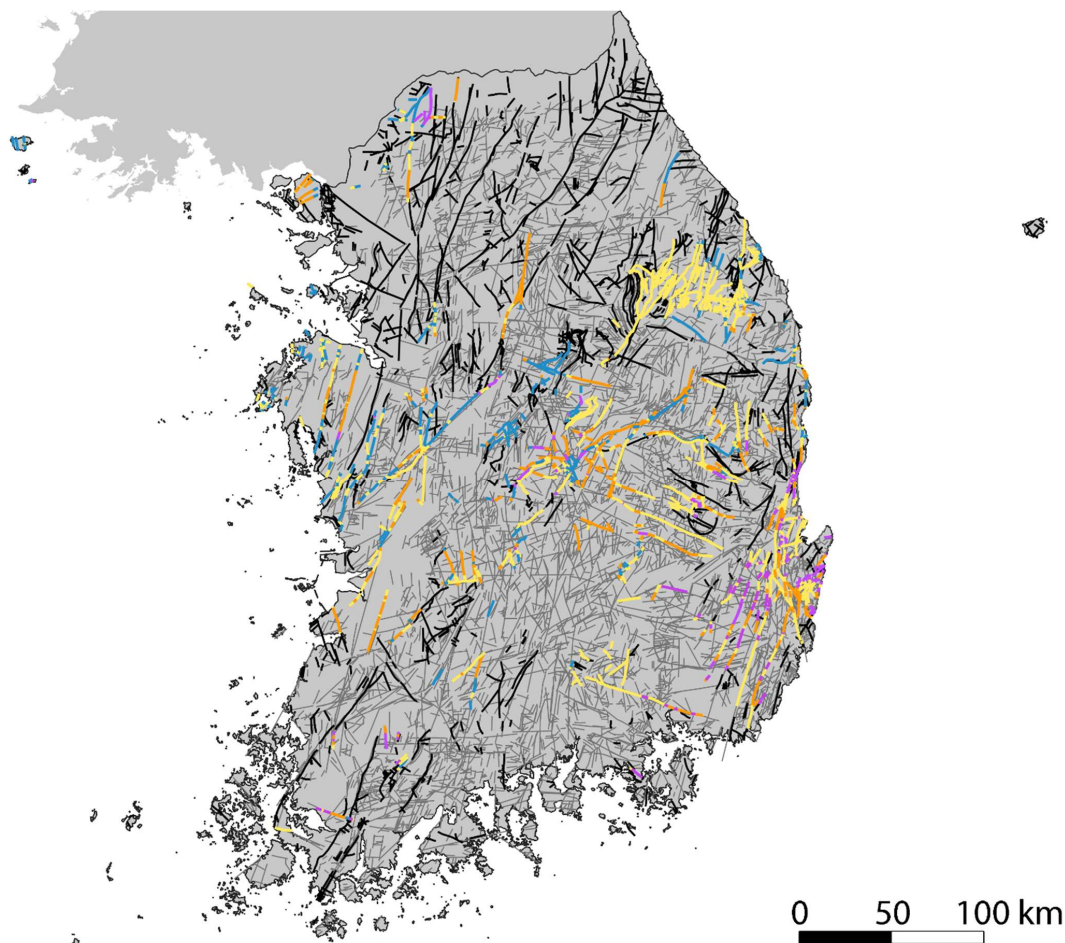
Lineaments (n=6,654)			
Fault zones outside earthquake-clusters (n=1,040)			
Potentially active fault zones (n=488, 1,153 segments)	**Intersected rock types**	**# of active fault segments**	**% of active fault segments**
	Granites	200	19.09
	Deformed Rocks (incl. schist and gneiss)	245	19.61
	Sedimentary Rocks	588	52.90
	Igneous Rocks	120	8.39

Figure 9. Potentially active fault zones distinguished by rock type (granites: orange, deformed rocks: blue, sedimentary rocks: yellow, and igneous rocks: pink lines). Fault zones which are not in the range of earthquake epicentres or clusters of these are shown as black lines and lineaments as grey lines. Note that slightly more than half of the fault zone segments (53 %) are hosted by sedimentary rock types, while Granites and deformed rocks host about 19 % each, and 8 % are hosted by igneous rocks.

Table 6. Active fault trace segments per Rock type distinguishing 4 rock types. Statistics of active fault trace segments distinguishing 11 rock types are shown in Appendix Table A5. The intersection of active fault traces and rock type polygons split the 488 active fault traces into 1,153 segments. (FaultsInEQclusters0.1contour_FaultsOnEpicenters_merged_uniques (n=488)_intersectWith_Rock(byRockTy_aggregated)_Collected_fgeo.shp, see Table A11)

440

Rock Types(aggregated)	Area km²	area_%	Total length of active fault segments	# of active fault segments	% of active fault segments	Average active fault segment length
	km²	%	km	#	%	km
Granites	29,095	29	928	200	19.09	4.64
Deformed Rocks (incl. schist and gneiss)	28,458	29	953	245	19.61	3.79
Sedimentary Rocks	28,891	29	2,571	588	52.90	3.44
Igneous Rocks	12,987	13	408	120	8.39	3.54
Sum	**99,431**	**100**	**4,859**	**1,153**	**100**	**3.85**

5. Discussion

5.1 Proof of concept: comparison of extracted and active faults already identified in previous studies

445 Since 2009 the National Emergency Management Agency (NEMA) of South-Korea made efforts to identify and investigate potentially active faults (Quaternary faults) throughout South-Korea in order to produce an active fault zone map of the country (NEMA 2012), which amongst others can be used for construction site planning (Galadini et al., 2012; He et al., 2022) and assessment of the seismic hazard in Korea (Park et al., 2021). The efforts of this "Active fault study" are still ongoing (Kim et al., 2020), and for this purpose experts utilise established and state-of-the-art methods comprising techniques ranging from

450 remote sensing, geomorphology, paleoseismology, Quaternary age dating and structural geology (e.g. Choi et al., 2014; Kim et al., 2023a and Kim et al., 2023b).

The method which we present in this work for determination of earthquake clusters and extraction of active faults, was developed without prior knowledge of previously mapped active fault zones. The comparison of our classification results (**Figures 7 and 9**) with the map of already known active fault zones in South-Korea (**Figure 10**) shows that our approach

455 using the seismic catalogue successfully identified 16 of 21 of the already known active fault zone traces (namely 1-6, 8 and 9 in parts, 12-14, 15-17 in parts, 20, 21), and added 473 previously unclassified fault zones in the areas of recent seismicity. Merely 5 of the fault surface traces (7, 10, 11, 18, 19) were missed by our analysis. Fault zones 8, 9 and 15-17 were captured in part due to discontinuities in the fault segmentation. The missed fault zones and those captured in part are located in the seismically less active SW- and NE-sectors of the peninsula.
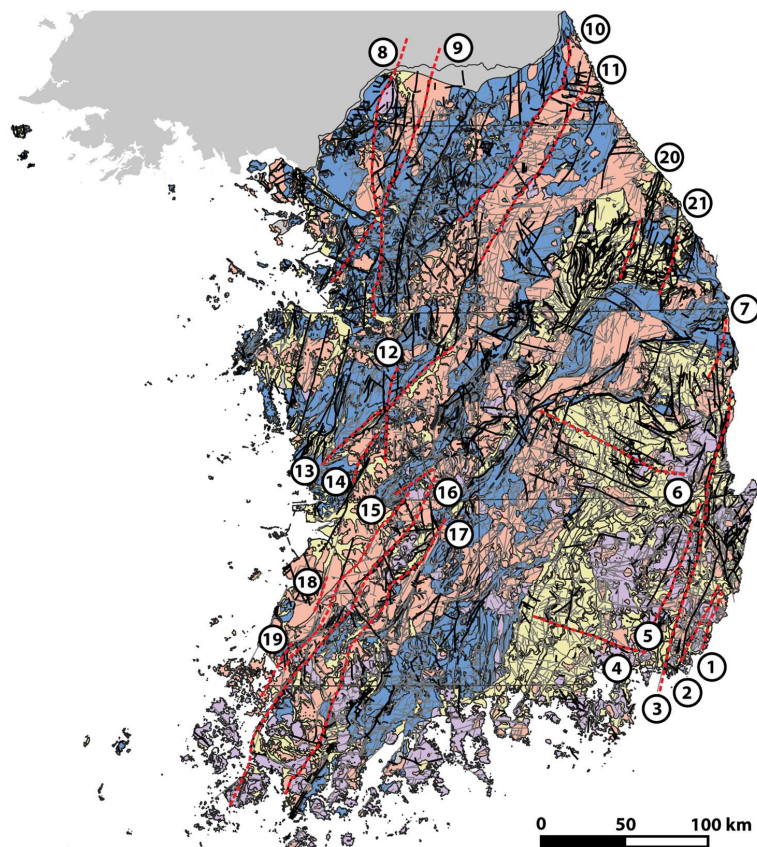
460

Figure 10. Known potentially active fault zones in South-Korea (stippled red lines adapted from NEMA 2012; respectively Park et al. 2021) on top of the geological map used in this work. Names of these faults are indicated in NEMA (2012).

In the following section we discuss our fault zone classification results along with the results of slip tendency analysis in order to provide more scientific background to the choice of the two rules we applied for extraction of the potentially active fault

465 zone dataset.

5.2 Slip tendency analysis

The slip tendency analysis is essential for assessing the potential of fault reactivation and seismicity occurrence. There are wide applications for slip evaluation, both on regional tectonic faults (e.g., Röckel et al., 2022) and site fractures (e.g., Moeck et al., 2003). Following Morris et al. (1996), the slip tendency (T_s) is defined as the ratio of resolved shear stress (τ) to resolved

470 normal stress (σ) acting on a fracture plane:

24

$$T_s = \frac{\tau}{\sigma}$$

$$\sigma = l^2 S_1 + m^2 S_2 + n^2 S_3$$

$$\tau = \sqrt{(s_1 - s_2)^2 l^2 m^2 + (s_2 - s_3)^2 m^2 n^2 + (s_3 - s_1)^2 l^2 n^2}$$

Where l, m and n are the direction cosines of the joint plane normal with respect to the principal stresses, S_1, S_2 and S_3, respectively.

When the value of slip tendency is greater than the coefficient of fracture friction, the slip occurs. The in-situ stress tensor and fault orientation are the relevant parameters for calculating slip tendency. When the pore pressure p_p is taken into account, the effective normal stress (σ_{eff}) is used for calculation.

$$\sigma_{eff} = \frac{\tau}{\sigma - P_P}$$

Previous studies investigating slip tendency in Korea focused on subsets of the fault zones on the Peninsula, such as e.g. was done by Park et al. (2006) for Quaternary faults in SE-Korea. Here we provide the first slip tendency analysis covering the entire peninsula.

For our analysis we used the present-day stress state deduced from earthquake focal mechanism inversions by Soh et al. (2018). The inversion provides both tectonic stress orientations and magnitudes over the Korean Peninsula. The prevailing stress regime is strike-slip and the maximum horizontal principal stress (S_{Hmax}) is oriented ENE-WSW consistently throughout the whole country. The variation of stress magnitudes is significantly bigger than the orientation. Our analysis simply adopted intermediate values of stress estimation. The S_{Hmax} is oriented 75° from the north and the S_{Hmax}/S_v (vertical principal stress) ratio is 2.0. The S_{hmin}/S_v ratio is 0.7. The vertical principal stress is treated as the overburden of host rock. The hydrostatic pore pressure is considered without overpressure condition and the P_p/S_v ratio is 0.25, assuming the rock density is 2,500 kg/m³.

As shown in **Figure 11**, surface traces of fault zones were determined and the surface trace of a fault can provide fault dip direction at the surface but no dip angle information. We considered three scenarios of dip angle. For the slightly dipped (sub-horizontal) scenario, a dip angle of 15° was assigned, and dip angles of 45° and 75° were used for the moderately dipped and highly dipped (sub-vertical) scenarios, respectively.

Using above mentioned stress and fault orientation data, the slip tendency of potentially active fault (yellow and red lines in **Figure 7**) zones was obtained. As seen in **Figure 11**, the impact of fault dip angle on slip tendency is significant. The slip tendency generally increases with the dip angle for the current study, which is consistent with the fact that fractures optimally

25

oriented for slip are highly dipped for the strike-slip stress regime (Xie & Min, 2016). For the highly dipped scenario, the slip potential for most faults, especially those with the strike subparallel to the maximum horizontal stress (75° from the north), is high and the magnitude of slip tendency can even be over 0.6. According to Byerlee's compilation (Byerlee, 1978), the frictional coefficient of rock fractures and faults ranges from 0.6 to 1.0. The slip occurs when the value of slip tendency is greater than the frictional coefficient. Results of slip tendency calculation show that the slip and associated seismicity are likely to happen for the faults with a high dip angle. This analysis not only agrees with the rules of identification of potentially active fault zones, faults either intersecting an earthquake cluster or in the vicinity of an earthquake epicentre, but also indicates the potential active fault zones in South Korea are likely to be highly dipped (sub-vertical).
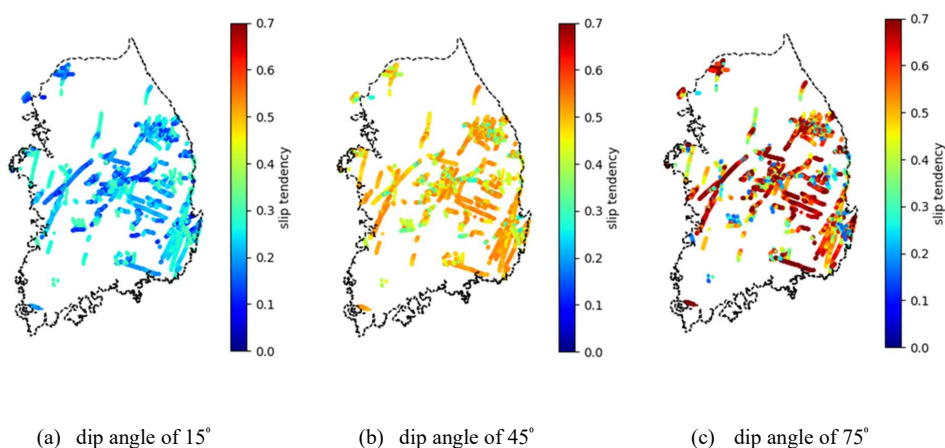
(a) dip angle of 15°   (b) dip angle of 45°   (c) dip angle of 75°

Figure 11. Slip tendency of potentially active fault zones: (a) slightly dipped scenario, (b) moderately dipped scenario and (c) highly dipped scenario

The slip tendency of fault zones outside of EQ-clusters (black lines in **Figure 8**) was also analysed and the results are presented in **Figure 12**. The impact of fault dip angle on slip tendency is similar as the case of potential active zones and the slip tendency generally increases with the dip angle, mainly because of the strike-slip stress regime. It is noticed that the faults with their strikes subparallel to the maximum horizontal stress (75° from the north) can have high slip potential with increasing dip angle even though they are outside of EQ-clusters and historically inactive regarding the seismicity. The low historical seismicity may reflect these faults are less dipped than the seismically active faults. Besides the fault dip angle condition, the low historical seismicity may also be induced by the field stress variation. According to Soh et al. (2018), southeastern South Korea has bigger magnitudes of S_{Hmax} and S_{hmin} than those of other regions of South Korea, and their differences are also larger in southeast South Korea. The seismically active fault zones are mainly in the southeast of South Korea, which is consistent with the larger deviatoric stress condition in the southeast, while most of historically inactive faults are located in the north and southwest of South Korea where there is less deviatoric stress.

(a) dip angle of 15°   (b) dip angle of 45°   (c) dip angle of 75°
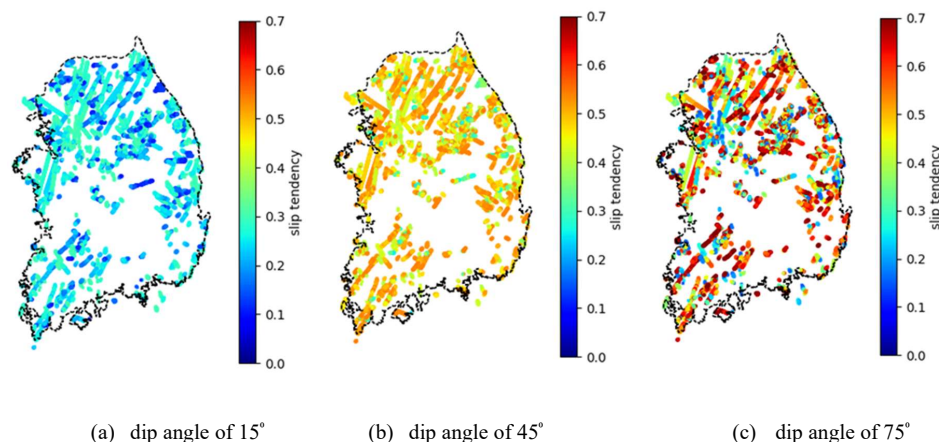
Figure 12. Slip tendency of fault zones outside of EQ-clusters: (a) slightly dipped scenario, (b) moderately dipped scenario and (c) highly dipped scenario

520   Taking above findings into account, in the next section we will take a look at different fault zone buffering approaches and develop a strategy for the definition of safety distances around the potentially active and the inactive fault zones on the Korean Peninsula.

5.3 Defining Safety Distances around fault zones

Apart of determining whether fault zones are active or not, safety distances have to be assigned around fault zones (e.g. He et

525   al., 2022) and for this purpose the areas of corresponding damage zones have to be estimated in order to ascertain that the confinement functions of a repository are not lost due to nearby fault activity or by perturbations such as increased water, gas and contaminant permeability due to fault displacement. This is true for both currently active and inactive faults. Different countries have developed different approaches to address this issue in their site search procedures taking into account the containment quality of the host rocks and seismic risk to be expected at relevant time scales. In this study, we prepared buffer

530   zones on the fault zones of the South-Korean dataset according to the strategies of Japan (NUMO 2004; NUMO 2017), Germany (BGE 2022) and Sweden (SKB 2000; SKB 2004), which represent three endmembers in this respect. The buffering approaches applied in these three countries have in common that the repository is to be placed in an intact and mechanically stable crustal block which is not dissected by large-scale fractures such as regional faults.

In order to exclude fault activity affecting containment, in Japan for example it was decided to take the width of the damage

535   zone potentially impacted by fault activity to be about 1/100 of the length of the behavioural segments or of seismogenic faults (NUMO 2017). This conservative choice was made based on the results of Ogata and Honsho (1981), according to whom the width of the damage zone is within about 1/350 to 1/150 of the fault length. Such variable distance buffers are readily applied in the Q-GIS using short expressions such as **$length/100** in the Q-GIS buffer tool. In this work we present length/100-buffers

and length/50-buffers applied to the South-Korean dataset (**Figures 13 and 14**) and quantify the spatial extent of these in each

540   of the rock types by means of calculating the overlap between buffers and rock type polygons (**Tables 7 and 8**).
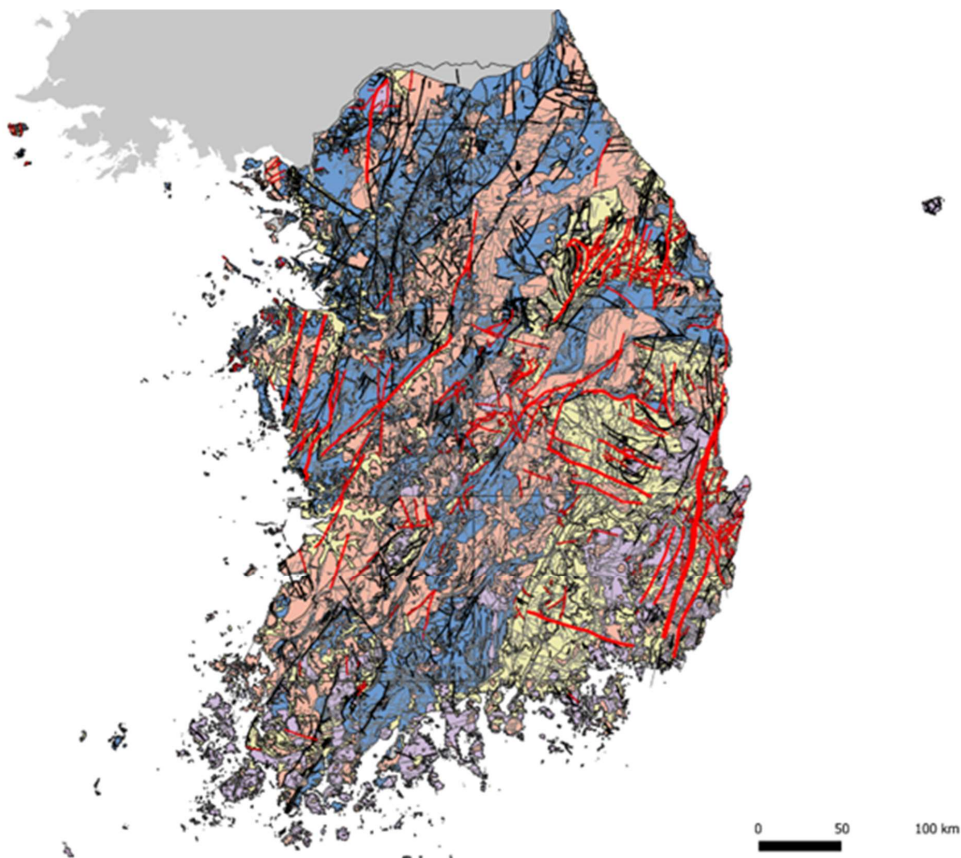
Figure 13. Potentially active fault zones in South-Korea buffered by a safety distance zone (red polygons) corresponding to fault length divided by 100 according to the Japanese approach (for dataset description see Table A11).

Table 7. Areal statistics of the areas covered by the fault-length/100-buffer drawn around faults that touch or intersect an earthquake
545   **cluster in each of the rock types in the geological map of South-Korea. The entire fault-length/100-buffer area covers 2.65 % of the onshore portion of South-Korea.**

Rock Units (aggregated)	Area km^2	Area %	Faults In EQ-clusters L/100-buffer area		
	km^2	%	m^2	km^2	%
Granites	29,095	29	253,501,768	254	1
Deformed Rocks (incl. schist and gneiss)	28,458	29	337,676,598	338	1

28

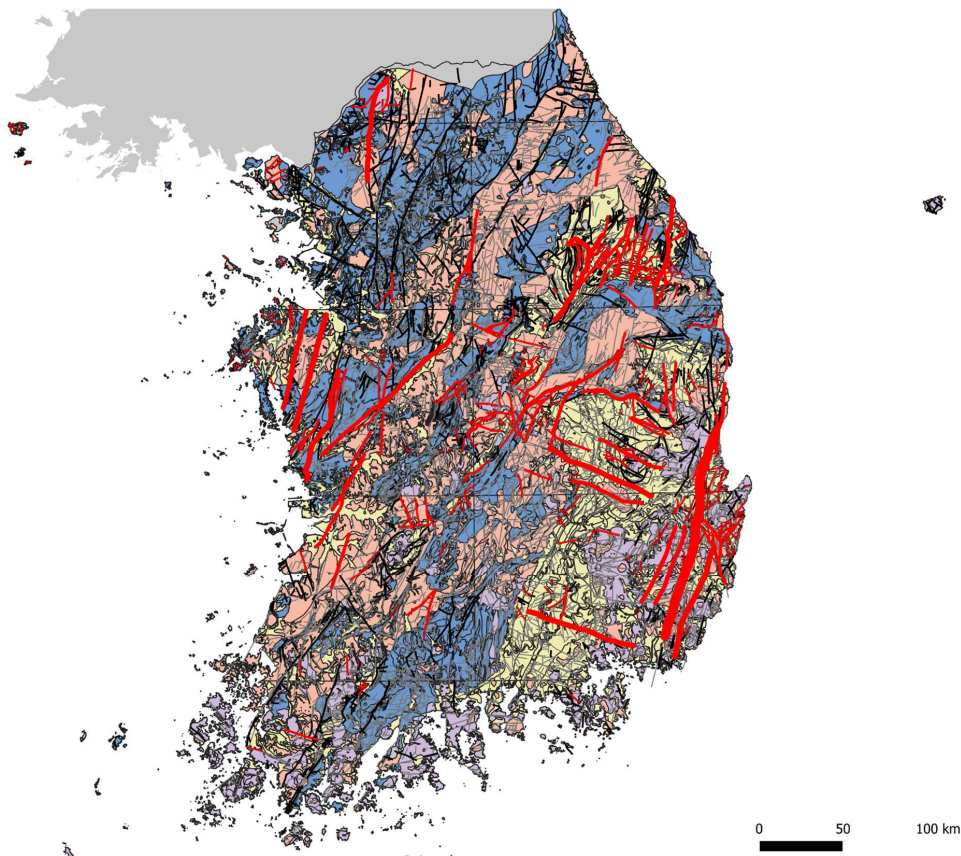|					
Sedimentary Rocks	28,891	29	1,184,300,465	1,184	4
Igneous Rocks	12,987	13	861,344,053	861	7
Sum	**99,431**	**100**	**2,636,822,885**	**2,637**	**2.65**

Figure 14. Potentially active fault zones in South-Korea buffered by a fault length/50 safety distance zone (red polygons), doubling the excluded area in comparison to the Japanese approach(for dataset description see Table A11).

550   **Table 8. Areal statistics of the areas covered by the fault-length/50-buffer drawn around faults that touch or intersect an earthquake cluster in each of the rock types in the geological map of South-Korea. The entire fault-length/50-buffer area covers 5.26 % of the onshore portion of South-Korea.**

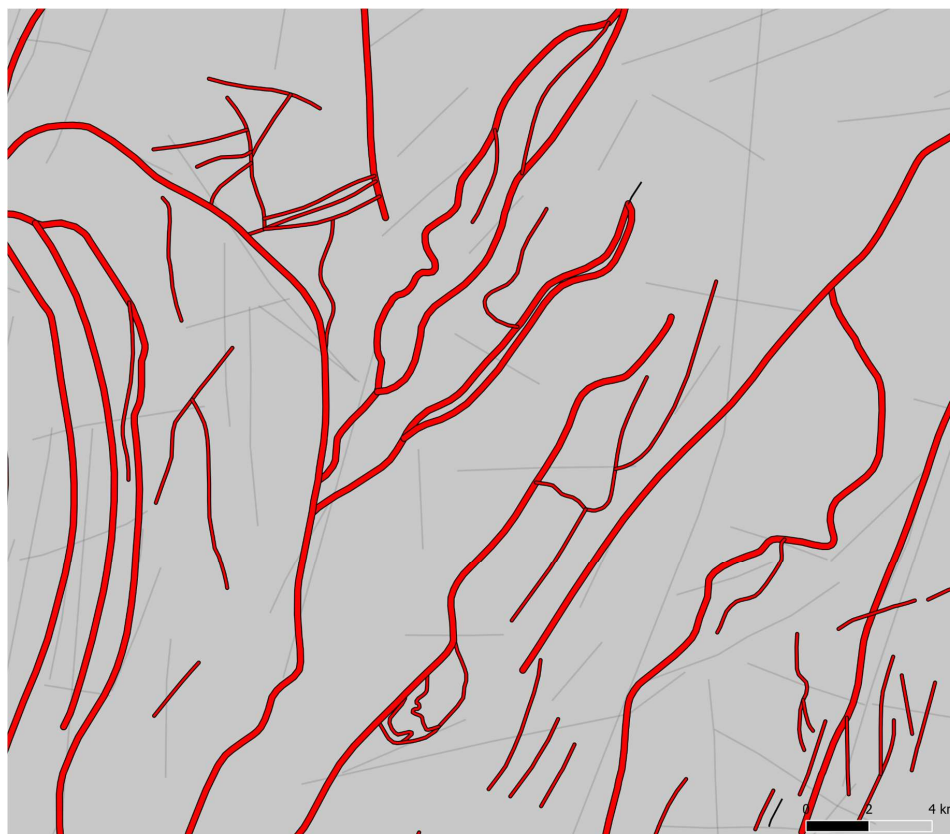| Rock Units (aggregated)	Area km²	Area %	Faults In EQ-clusters L/50-buffer area		
	km²	%	m²	km²	%

Granites	29,095	29	506,166,776	506	2
Deformed Rocks (incl. schist and gneiss)	28,458	29	685,433,598	685	2
Sedimentary Rocks	28,891	29	2,319,456,242	2,319	8
Igneous Rocks	12,987	13	1,723,780,796	1,724	13
Sum	**99,431**	**100**	**5,234,837,413**	**5,235**	**5.26**

In Sweden, SKB (Svensk Kärnbränslehantering AB) has chosen to classify fault zones according to length (size) using the designations "regional fault zones", "local major fault zones", "local minor fault zones" and "fractures" (e.g. SKB 2000, SKB

555 Technical Report TR-00-12; SKB 2004, SKB Report R-04-17). Considering that the repository in Korea will be built in granitic rock as is done in Sweden, and as is also foreseen in the Korean Reference HLW Disposal System, Korean scientists adopted this classification and the rules for definition of corresponding respect distances (Lee et al. 2007; Choi et al., 2008). Choi et al. (2013) e.g. proposed to apply 100 m wide buffer zones with respect to the repository area on regional fault zones exceeding 10 km length, 50 m wide buffer zones with respect to the disposal tunnels around local major fault zones having lengths

560 between 1 and 10 km, and 5 m respect distances around local minor fault zones (being 10 m to 1 km long) to avoid deposition hole locations (see **Table 9**, modified from Choi et al 2013).

Table 9. Classification of the fault zones, their approximate lengths and damage zone widths, and safety distances to be defined according to Choi et al. (2013).

Name of fault zone class	Length	Width	Safety Distance
Regional fault zones	> 10 km	> 100 m	100 m (to repository)
Local major fault zones	1–10 km	5–100 m	50 m (to disposal tunnels)
Local minor fault zones	10 m–1 km	0.1–5 m	5 m (to deposition holes)
Fractures	< 10 m	< 0.1 m	-

565 This type of buffering in principle does not require any prior knowledge of whether the faults are active or not, and thus in our example we apply the buffer widths to the entire fault zone dataset of Korea (**Figure 15**) using the conditional expression **if ("LENGTH_M">10000, 100, if ("LENGTH_M"<1000, 5, 50))**, and quantify the area captured by the buffer zones in each of the rock types distinguished in the simplified geological map (**Table 10**).

Figure 15. Excerpt map of both, active and inactive fault zones in South-Korea buffered according to the Swedish approach, as described in Table 9: Regional faults (>10 km length) by 100-m-buffers, Major faults (1-10 km length) by 50-m-buffers, and Minor faults (10 m - 1 km length) by 5-m-buffers (red polygons). For dataset description see Table A11.

Table 10. Areal statistics of the areas covered by the 100-m- , 50m-, and 5m-buffers drawn around both active and inactive regional, major and minor faults, respectively, in each of the rock types in the geological map of South-Korea. The entire buffer area covers 0.12 % of the onshore portion of South-Korea.

Rock Types (aggregated)	Area km^2	Area %	Faults buffered by 100m- , 50m-, and 5m-buffers		
	km^2	%	m^2	km^2	%
Granites	29,095	29	22,757,772	22.76	0.078
Deformed Rocks (incl. schist and gneiss)	28,458	29	32,702,577	32.70	0.115
Sedimentary Rocks	28,891	29	53,229,015	53.23	0.184

31

Igneous Rocks	12,987	13	8,085,738	8.09	0.062
Sum	**99,431**	**100**	**116,775,102**	**116.78**	**0.117**

The buffering method described by Germany's Federal Agency for final disposal BGE (2022) in contrast amongst others distinguishes between supra-regional and regional faults, which are to be excluded, if they can be proven active within the past 34 Ma years, as defined in the exclusion criterion "active fault zones" in Germany's Site Selection Act (StandAG 2017):

"The "conditionally favourable area" of supra-regional fault zone buffers is based on the rating groups of the indicators
580 *according to the Site Selection Act (StandAG 2017) and their width is to be given as 3 km. The "conditionally favourable area", which should be placed around regional faults, is based on the specifications for the safety distance of the exclusion criterion "active fault zones" and is at least 1 km"* according to the draft of the Site Selection Act (BT-Drs.18-11398 2017, p. 68).

In order to better characterise the deformation history of rock units, BGE furthermore investigates 2) the large-scale tectonic overprint of tectonic provinces and 3) more local diffuse tectonic overprint, which however will not be topic in this paper, due
585 to lack of information in that respect at the current stage of the South-Korean site search. The rating of supra-regional and regional fault zones as described by BGE (2022) and corresponding respect distances around affected areas along surface ruptures are displayed in the table below (**Table 11**).

Table 11: Rating groups of the supra-regional and regional fault zones according to BGE (2022, Table 53). The width of the conditionally favourable and unfavourable buffer zones that are to be placed around supra-regional and regional fault zones is
590 **given.**

Classification of fault zones	Rating groups		
	favourable	conditionally favourable	unfavourable
Supra-regional fault	Over 3km	Up to 3 km	Up to 100m
Regional Fault	Over 1km	Up to 1 km	Up to 100m

Here, we first present the application of simple 1-km-buffers on all active faults in the South-Korean dataset (**Figure 16**), and then in a second approach adopt the distinct treatment of large-scale fault zones by length and application of respective respect distances (1 and 3 km buffers, see **Figure 17**). Here we chose to apply the 3-km-buffer not only to the active supra-regional faults but also to the active regional faults (i.e. all faults >10 km), and to apply the 1-km-buffer to all shorter fault zones
595 (compare with **Table 9**), using the conditional expression **if (LENGTH_km>10, 3, 1)** in the Q-GIS buffer-tool. Resulting overlaps between buffer and rock type areas for the two buffering-approaches are presented in **Tables 12 and 13**. Further examples of conditional buffering applying the expressions **if (LENGTH_km>50, 3, 1)**, **if (LENGTH_km>40, 3, 1)**, **if (LENGTH_km>30, 3, 1)**, and **if (LENGTH_km>20, 3, 1)** are presented in **Appendix Figures A7-A10**, along with corresponding areal statistics (**Tables A7-A10**) in order to demonstrate the areal effect of choosing different length-limits for
600 distinction between faults to be buffered with a 3 km respect distance zone and faults to be buffered by a 1 km respect distance.
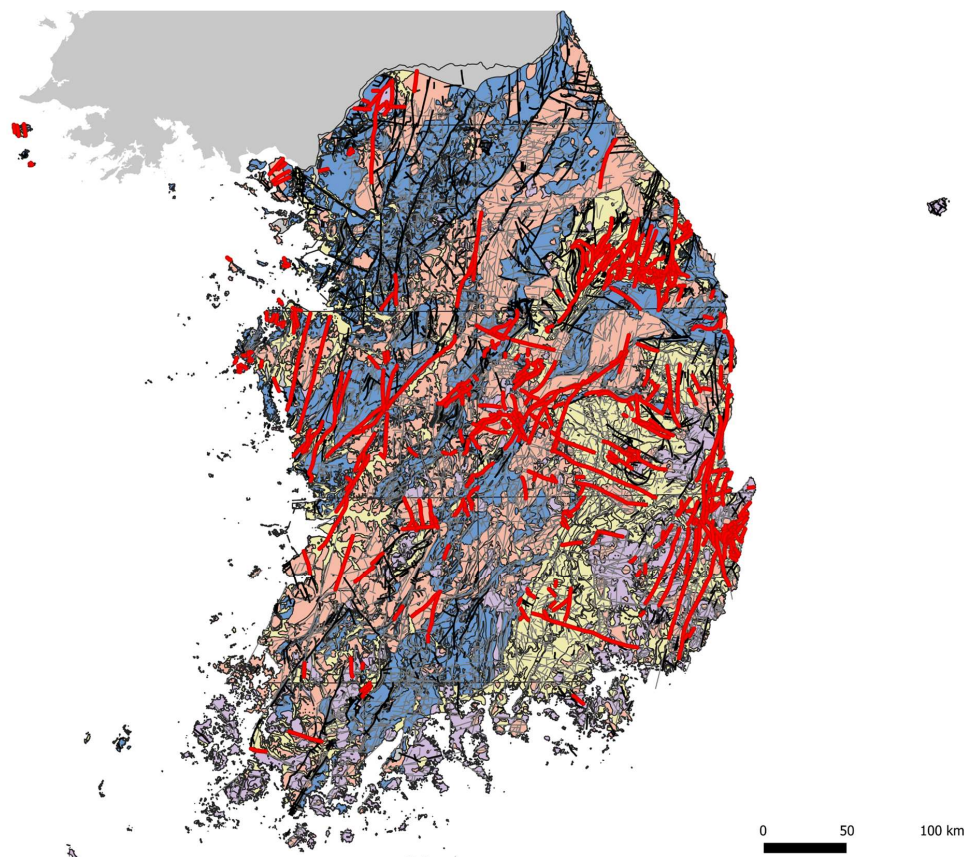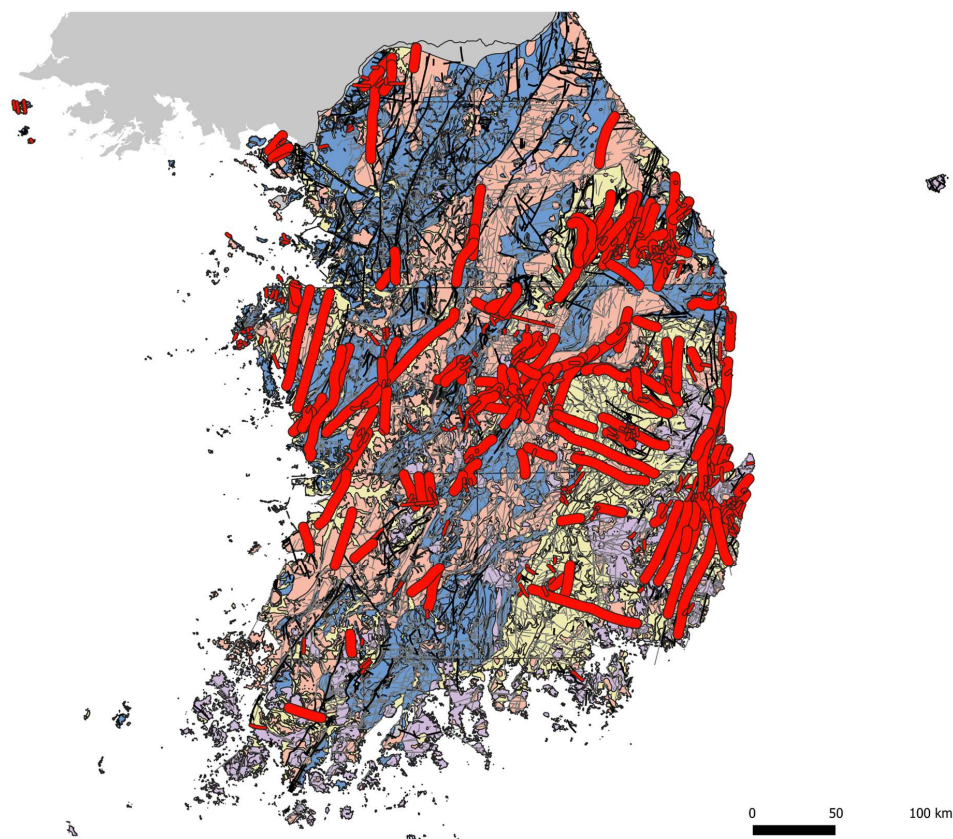
Figure 16. Potentially active fault zones in South-Korea buffered by a 1-km-safety-distance (red polygons) according to the German approach (for dataset description see Table A11).

Table 12. Areal statistics of the areas covered by the 1-km-buffer drawn around faults that touch or intersect an earthquake cluster in each of the rock types in the geological map of South-Korea. The entire 1-km-buffer area covers 9.29 % of the onshore portion of South-Korea, i.e. consuming 4 times more space than the Japanese-type Length/100-buffer (and twice as much as the Length/50-buffer).

Rock Types (aggregated)	Area km^2	Area %	Faults In EQ-clusters 1-km-buffer area		
	km^2	%	m^2	km^2	%
Granites	29,095	29	898,474,322	898	3
Deformed Rocks (incl. schist and gneiss)	28,458	29	1,368,748,562	1,369	5

33

Sedimentary Rocks	28,891	29	3,834,927,714	3,835	13
Igneous Rocks	12,987	13	3,136,853,233	3,137	24
Sum	**99,431**	**100**	**9,239,003,830**	**9,239**	**9.29**

Figure 17. Potentially active fault zones in South-Korea buffered by a 1-km- and a 3-km-safety buffer (red polygons), respectively, utilising a modification of the German buffering approach. Here, we distinguish supra-regional and regional fault zones by length (>10 km) from minor and major fault zones (<10 km). For dataset description see Table A11.

Table 13. Areal statistics of the areas covered by the 1-km- and 3-km-buffer drawn around faults shorter than, and faults longer than 10 km, respectively. that touch or intersect an earthquake cluster in each of the rock types in the geological map of South-Korea. The entire 1-km- and 3-km-buffer area covers 20.45 % of the onshore portion of South-Korea, i.e. adding 11.16 % to the 1-km-buffer area.

34

Rock Types (aggregated)	Area km^2	Area %	Faults In EQ-clusters 1&3km-buffer area(10kmLimit)		
	km^2	%	m^2	km^2	%
Granites	29,095	29	5,517,540,101	5,518	19
Deformed Rocks (incl. schist and gneiss)	28,458	29	4,116,479,680	4,116	14
Sedimentary Rocks	28,891	29	8,775,569,859	8,776	30
Igneous Rocks	12,987	13	1,924,726,786	1,925	15
Sum	**99,431**	**100**	**20,334,316,426**	**20,334**	**20.45**

Comparing the above presented examples of different buffering methods applied to the fault zones on the Korean Peninsula clearly shows the areal differences between the Japanese, German and Swedish approaches to exclude fractured bedrock areas from site search. The different choice of respect distance definitions for fault zones reflects the different reasoning and priorities

620   set by these countries based on the different geological settings and planning scientific rationale. Japan is similarly densely populated as Korea, i.e. has constrained usable area, and is located in a high seismicity region characterised by frequent large magnitude subduction zone earthquakes affecting the entire island (e.g. Mogi 1981), and thus their approach focuses on excluding areas based on the damage zone width which can be inferred from fault length (NUMO 2017), which would consume 3-5 % of the area on the Korean Peninsula (**Figures 13 and 14**). The seismicity in Germany generally is low with the exception

625   of some enhanced seismicity regions along the river Rhine and the Alps, and in Saxony-Thuringia area in the East of the country (e.g. Tyagunov et al., 2006). Therefore, their approach is to exclude areas around potentially active fault zones in the far-field (BGE 2022). This type of buffering, if applied to the fault zones on the Korean Peninsula would consume 10-20 % of the countries area (compare **Figures 16, 17 and Appendix Figures A7-A10**), making this the most conservative approach tested in this work. Sweden has rather low seismicity (e.g. Bath 1978), and their fault zone buffering approach was developed

630   for application at late stage in the site search procedure with focus on crystalline host rocks which typically are characterised by quite regularly occurring fracture patterns. The Swedish approach thus rather relies on an efficient engineered barrier system allowing to build the repository relatively close to regional and major fault zones. If applying this method in the Korean site search case, the resulting exclusion area would amount to less than 1 % of the Peninsula (**Figure 15**).

The choice of which buffering method is best suited for South-Korea depends on several factors, and in principle the buffering

635   techniques applied by Japan and Sweden, or those applied by Germany and Sweden could be combined to define exclusion areas for both active and inactive fault zones. Site search could be significantly sped up by using a very conservative exclusion approach defining wide respect distances from faults and seismically active regions, as e.g. is done by Germany. This would also help building trust in affected communities and the general public (Kim & Park, 2017; Schafmeister 2023). The authors of this work thus propose using 3-km-buffers applied both to potentially active supra-regional and regional fault zones (>10

640   km length), 1-km-buffers applied to major and minor fault zones (<10 km length) and further to apply 100-m-buffer zones to inactive regional faults (> 10 km length), 50-m-buffers to inactive major faults (1-10 km length), and 5-m-buffers to inactive

minor faults (10 m - 1 km length). This way, seismically active regions are spaciously excluded, placing the focus on less fractured terrain at early stage of site search, and inactive fault zones, which could be re-activated at time scales of hundreds to thousands of years (e.g. Stein et al. 2009; Calais et al., 2016), are taken into account as well.

645 **6. Conclusion**

Identification of potentially active fault zones is essential for the exclusion of areas not suited for disposal of high-level radioactive waste. In this work we provide a GIS-based workflow for the identification of potentially active fault zones based on the historical earthquake record, and provide a first quantitative areal assessment of exclusion zones around seismically active regions in South-Korea, and how much of the different host rock types are affected by these areas, distinguishing

650 Granites, deformed/metamorphic rocks, sedimentary rocks, and igneous rocks. Application of slip tendency analysis on potentially active fault zones corroborates the results of our classification, and furthermore enabled characterization of the subsurface geometry such as the dip of active and inactive fault systems. More specifically, the slip tendency analysis shows that most of the fault zones classified as potentially active in South-Korea are likely highly dipped.

Data availability

655 The geo-spatial datasets used and produced during the current study are available as electronic supplement to this work and from the corresponding authors on reasonable request.

Authorship contribution statement

Conceptualization of work was done by S. Bredemeyer, J.S. Yoon, and J.H. Lee. Data analysis and work-flow development in Q-GIS was carried out by S.B. and slip tendency analysis was performed by L. Xie. The manuscript was written by S.B.

660 and L.X. with the support of J.S.Y..

Declaration of Competing Interest

The authors declare that they have no known competing financial interests or personal relationships that could have inappropriately influenced the work reported in this paper.

Acknowledgements

(2021040101003C). Figures were produced in Q-GIS, Python and Adobe Illustrator. The University of California in Berkely is acknowledged for providing shapefiles containing the outlines of the administrative areas in Korea.

Appendix

670 **Table A1. Faults per Rock type distinguishing 11 rock types. Total area sizes of rock types are compared to sum of lengths of all fault segments in each rock type, # of fault segments per rock type, % of faults per rock type, average fault segment lengths per rock type. Further, the earthquake magnitudes the faults in each rock type are capable of according to the surface rupture length to moment magnitude relationship were determined by Wells and Coppersmith (1994). (Line segments: Data_20230512-fault_intersectwith_Rock(byRockTY_aggregated)_Collected_fgeo.shp, see Table A11)**

Rock types (detail)	Area km²	Area %	Sum of fault segment Lengths	# of fault segments	% of fault segments	Average fault segment Length	Average EQ-Magnitude (WC94)
	km²	%	km		%	km	M
Schist and gneiss	17,518	17.62	1,785	441	15.23	4.05	5.97
Granite	29,095	29.26	2,255	551	19.25	4.09	6.04
Other igneous rocks	7,078	7.12	591	235	5.04	2.51	6.06
Other sedimentary rocks	15,814	15.90	2,926	683	24.97	4.28	5.91
Granitic gneiss	6,994	7.03	724	240	6.18	3.02	6.03
Quarternary strata	8,917	8.97	1,322	404	11.28	3.27	6.06
Flow area	1,235	1.24	178	173	1.52	1.03	6.20
Limestone	2,324	2.34	837	230	7.14	3.64	5.94
Other metamorphic rocks	3,946	3.97	826	267	7.05	3.09	5.84
Sandstone and mudstone	602	0.61	52	20	0.44	2.58	6.07
Tuff	5,909	5.94	220	89	1.88	2.48	5.92
Sum	**99,431**	**100**	**11,715**	**3,333**	**100**	**3.51**	**6.00**

675

Table A2. Lineaments per rock type distinguishing 11 rock types. Total area sizes of rock types are compared to sum of lengths of all lineament segments in each rock type, # of lineament segments per rock type, % of lineaments per rock type, and average lineament segment lengths in each rock type are indicated. (Line segments: Data_20230512-lineament_intersectwith_Rock(byRockTY_aggregated)_Collected_fgeo.shp, see Table A11)

Rock types (detail)	Area km²	Area %	Sum of lineament segment Lengths	# of lineament segments	% of lineament segments	Average lineament segment Length
	km²	%	km	#	%	km
Schist and gneiss	17,518	17.62	6,227	1,723	15.22	3.61

Rock Type	Area km²	Area %				
Granite	29,095	29.26	12,451	3,086	30.44	4.03
Other igneous rocks	7,078	7.12	2,471	1,057	6.04	2.34
Other sedimentary rocks	15,814	15.90	7,919	2,205	19.36	3.59
Granitic gneiss	6,994	7.03	2,833	970	6.92	2.92
Quarternary strata	8,917	8.97	3,105	1,202	7.59	2.58
Flow area	1,235	1.24	507	496	1.24	1.02
Limestone	2,324	2.34	959	377	2.34	2.54
Other metamorphic rocks	3,946	3.97	2,131	677	5.21	3.15
Sandstone and mudstone	602	0.61	210	82	0.51	2.56
Tuff	5,909	5.94	2,091	596	5.11	3.51
Sum	**99,431**	**100**	**40,903**	**12,471**	**100**	**3.28**

680

Table A3. Number of earthquake occurrences in each rock type distinguishing 11 rock types.

Rock Types (detail)	Area km²	Area %	# of epicentres in rock type polygons (weighted by scale)	# of epicentres in rock type polygons	% of epicentres in rock type polygons
Schist and gneiss	17,518	18	193	79	9.31
Granite	29,095	29	526	212	24.97
Other igneous rocks	7,078	7	154	63	7.42
Other sedimentary rocks	15,814	16	478	196	23.09
Granitic gneiss	6,994	7	57	22	2.59
Quarternary strata	8,917	9	387	156	18.37
Flow area	1,235	1	12	5	0.59
Limestone	2,324	2	60	25	2.94
Other metamorphic rocks	3,946	4	81	32	3.77
Sandstone and mudstone	602	1	3	1	0.12
Tuff	5,909	6	143	58	6.83
Sum	**99,431**	**100**	**2,093**	**849**	**100**

Table A4. Rock type area covered by the onshore earthquake clusters obtained from the heatmap map contours shown in Figure 8. Distinguished are 11 rock types.

Rock Types (detail)	Area km²	Area %	KDE-Rad0.1 area km²	KDE-Rad0.1 area % of country	KDE-Rad0_1 area % of rock type

38

Schist and gneiss	17,518	18	2,409	13.75	12.01
Granite	29,095	29	6,626	22.77	33.03
Other igneous rocks	7,078	7	1,680	23.74	8.38
Other sedimentary rocks	15,814	16	3,632	22.97	18.11
Granitic gneiss	6,994	7	1,131	16.17	5.64
Quarternary strata	8,917	9	1,728	19.38	8.61
Flow area	1,235	1	220	17.82	1.10
Limestone	2,324	2	808	34.77	4.03
Other metamorphic rocks	3,946	4	977	24.75	4.87
Sandstone and mudstone	602	1	19	3.15	0.09
Tuff	5,909	6	830	14.05	4.14
Sum	**99,431**	**100**	**20,058**	**20.17**	**100.00**

685

Table A5. Active fault trace segments per Rock type distinguishing 11 rock types. (Line segment product: FaultsInEXclusters0.1contour_FaultsOnEpicenters_merged_uniques_(n=488)_intersectWith_Rock(byRockTy_aggregated)_Collected_fgeo.shp, see Table A11)

| Rock Types (detail)	Area km²	Area %	Total length of active fault segments	# of active fault segments	% of active fault segments	Average active fault segment length
	km²	%	km	#	%	km
Schist and gneiss	17,518	17.62	477	110	9.82	4.34
Granite	29,095	29.26	928	200	19.09	4.64
Other igneous rocks	7,078	7.12	313	95	6.45	3.30
Other sedimentary rocks	15,814	15.90	1,461	271	30.07	5.39
Granitic gneiss	6,994	7.03	211	62	4.34	3.40
Quarternary strata	8,917	8.97	566	141	11.66	4.02
Flow area	1,235	1.24	54	69	1.11	0.78
Limestone	2,324	2.34	480	103	9.87	4.66
Other metamorphic rocks	3,946	3.97	265	73	5.45	3.63
Sandstone and mudstone	602	0.61	9	4	0.19	2.36
Tuff	5,909	5.94	94	25	1.94	3.78
Sum	**99,431**	**100**	**4.859**	**1,153**	**100**	**4.21**

690

39
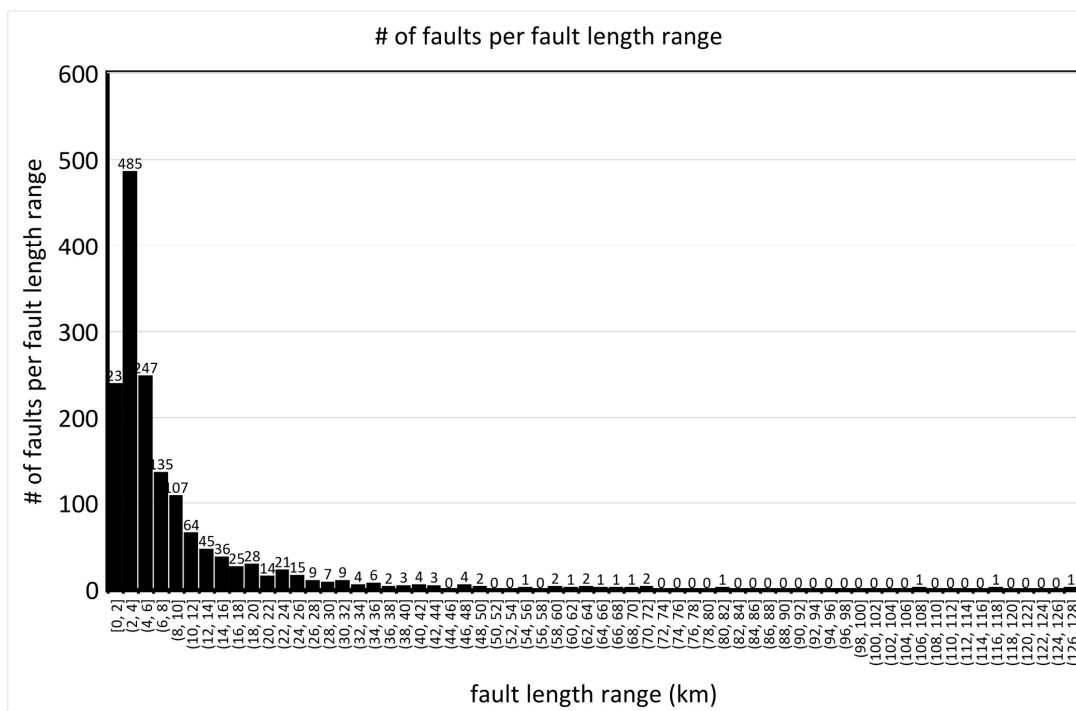
Figure A1. Fault length histogram (2 km bins) of the 1,528 fault zones in South-Korea. Data values, i.e. numbers of faults per fault length range are indicated on top of each of the bars.
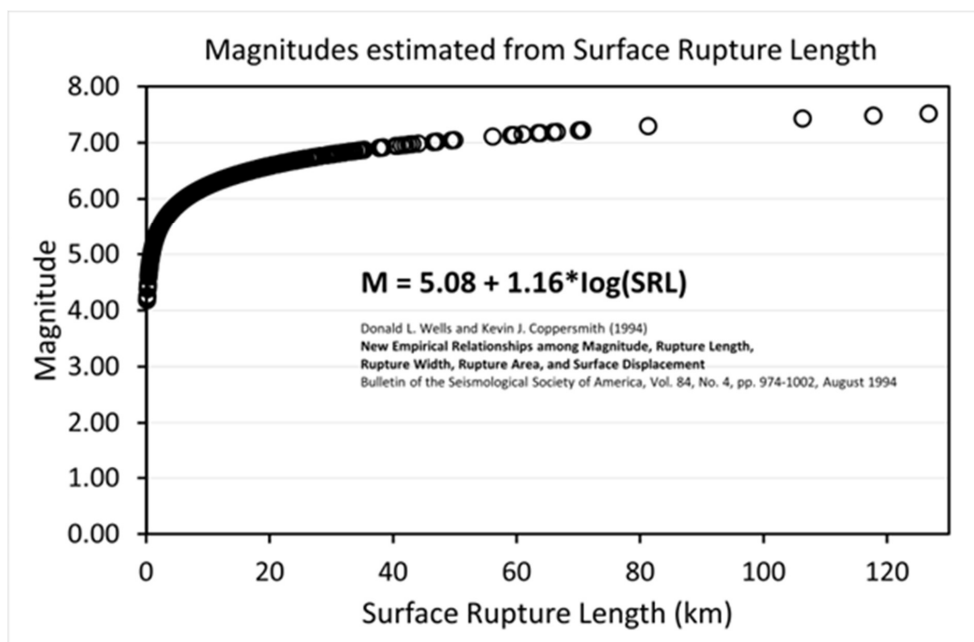
Figure A2. Magnitudes estimated from surface rupture length according to the empirical relationship determined by Wells and Coppersmith (1994). Most of the faults analysed here, would be capable of producing earthquakes in the Magnitude range M5-7, which would be sufficiently large to damage or even rupture a canister designed for HLW disposal.

695
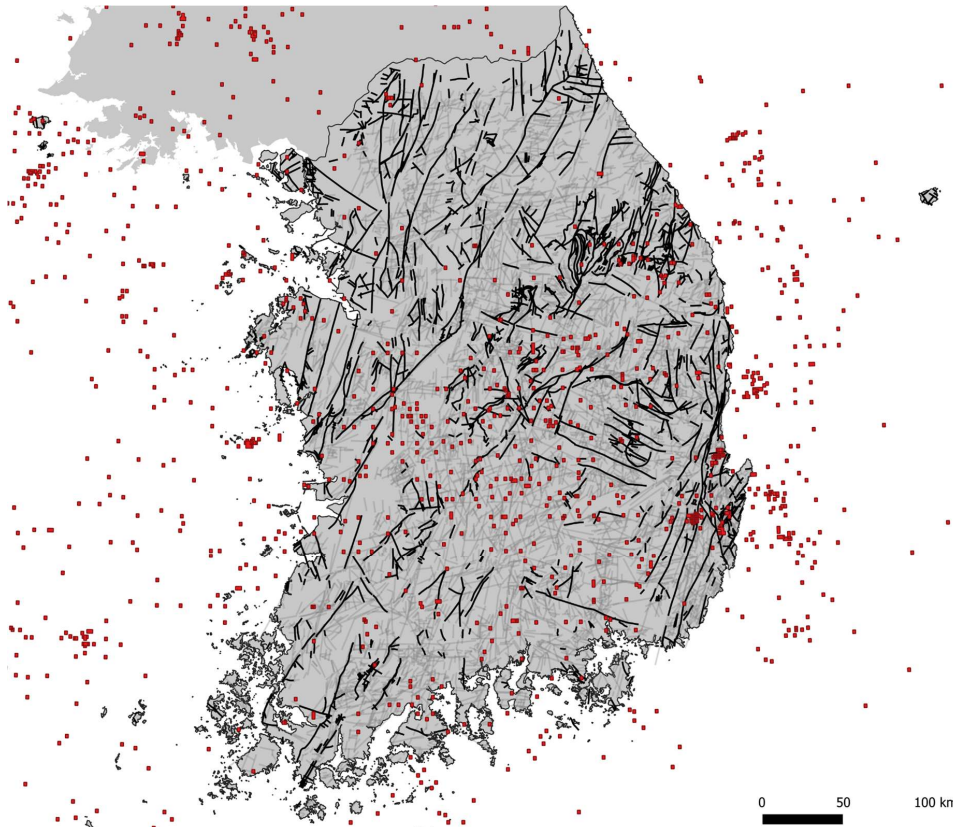
Figure A3. Polygons obtained from the Earthquake-density heatmap used for colocation of epicentres and faults. Both, kernel radius and pixel size used for kernel density estimation (KDE) from the historical earthquake record in and around South-Korea between 1991 and 2023 are 1 km. (Polygon products: PolygonizedKoreaEQheatmapKDE0.01degPxSize0.01.shp, PolygonizedKoreaEQheatmapKDE0.01degPxSize0.01_geometry_mainland.shp; obtained from Raster image product: KoreaEQ_HeatmapKDE_Radius0.01degPxSize0.01.tif, see Table A11)
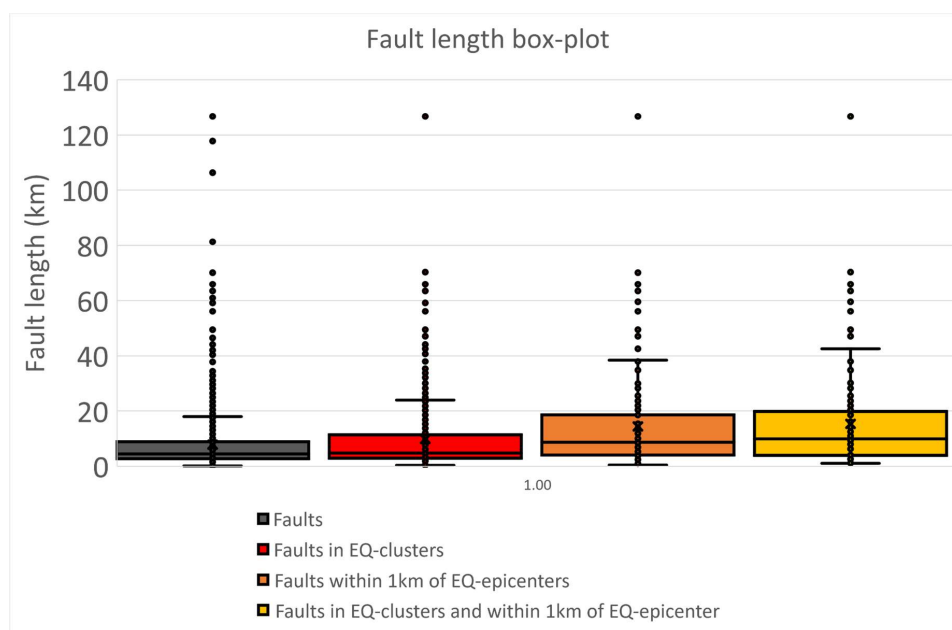
700

705
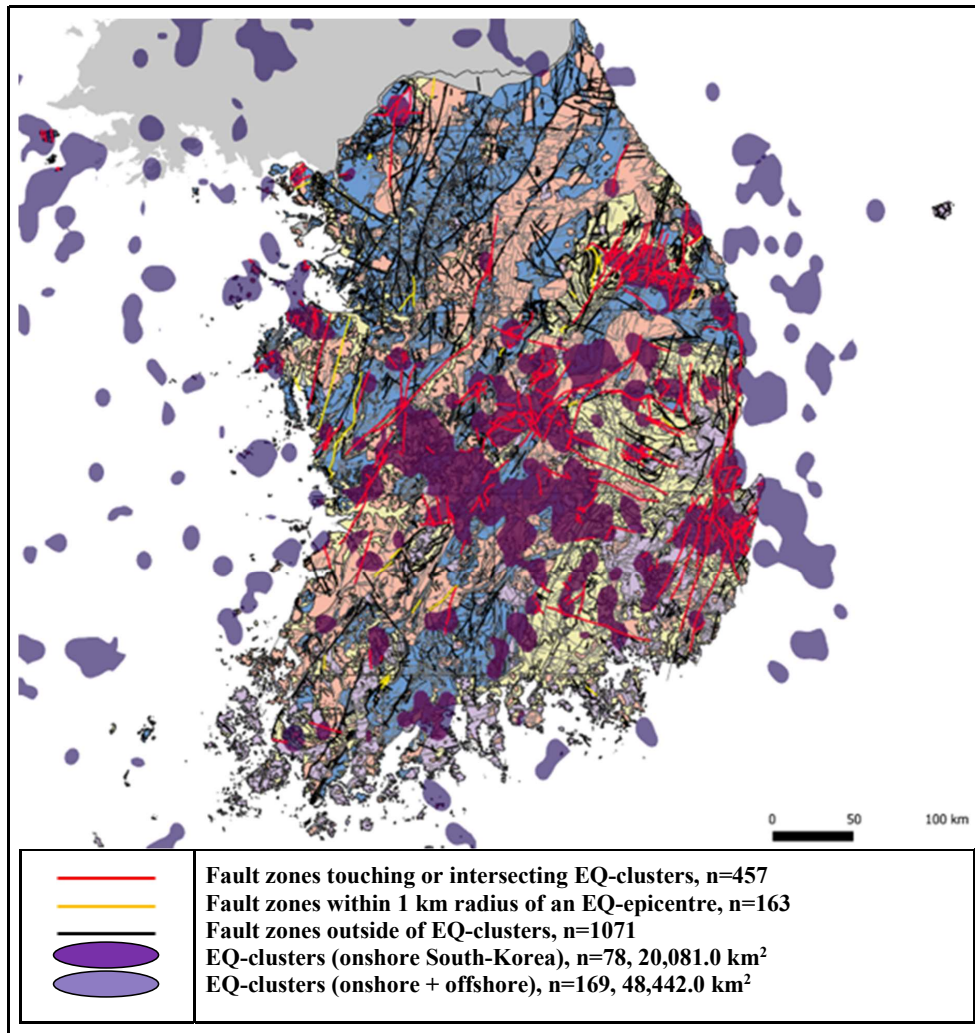
Figure A4. Results of the fault zone classification on top of determined earthquake epicentre clusters onshore and offshore South-Korea and distinguished rock types (granites, deformed rocks, sedimentary rocks and igneous rocks). Fault zones touching or intersecting earthquake clusters are displayed by red lines, fault zones within 1 km radius of an earthquake epicentre are shown as yellow lines.

710

Table A6. Length statistics of the entire fault dataset and the two identified groups of faults classified as potentially active, and the intersection of the two groups. The Table contents are graphically displayed in Appendix Figure A5 below.

| Fault Length statistics (km)	range	Mean	Median	StDev	Sum
Faults, n = 1528	0.16 - 126.71	7.81	4.42	10.30	11,941.06
Faults in earthquake-clusters, n = 457	0.28 -126.71	9.89	4.73	12.83	4,520.73
Faults within 1km of earthquake-epicentres, n = 163	0.47 - 126.71	14.43	8.71	17.19	2,352.08
Faults within 1km of earthquake-epicentres and in earthquake-clusters, n = 128	1.04 -126.71	15.35	9.89	17.48	1,964.76

715

Figure A5. Boxplot showing the fault length statistics of the 4 fault groups distinguished in Table A1.
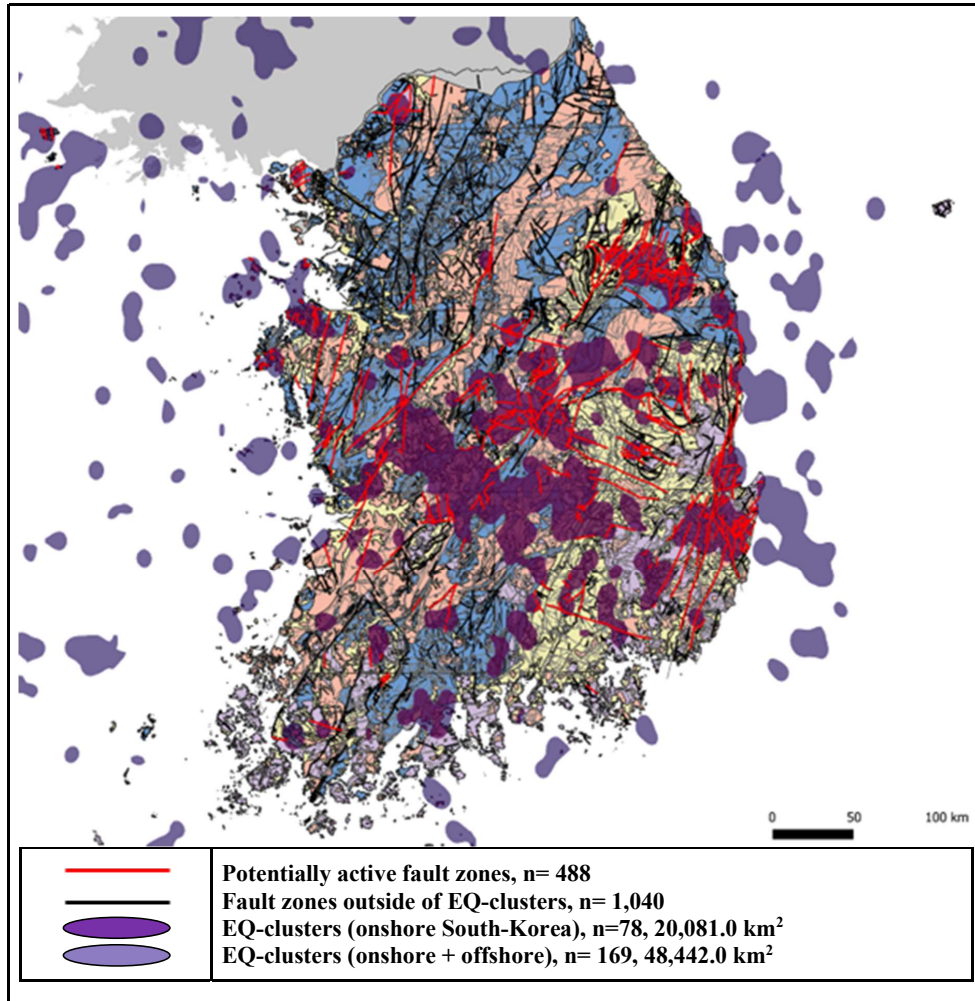
Figure A6. Results of the fault zone classification on top of determined earthquake epicentre clusters onshore and offshore South-Korea and distinguished rock types (granites, deformed rocks, sedimentary rocks and igneous rocks). Potentially active fault zones are displayed by red lines, surface traces of fault zones which are not in the range of earthquake epicentres or clusters of these are shown as black lines.
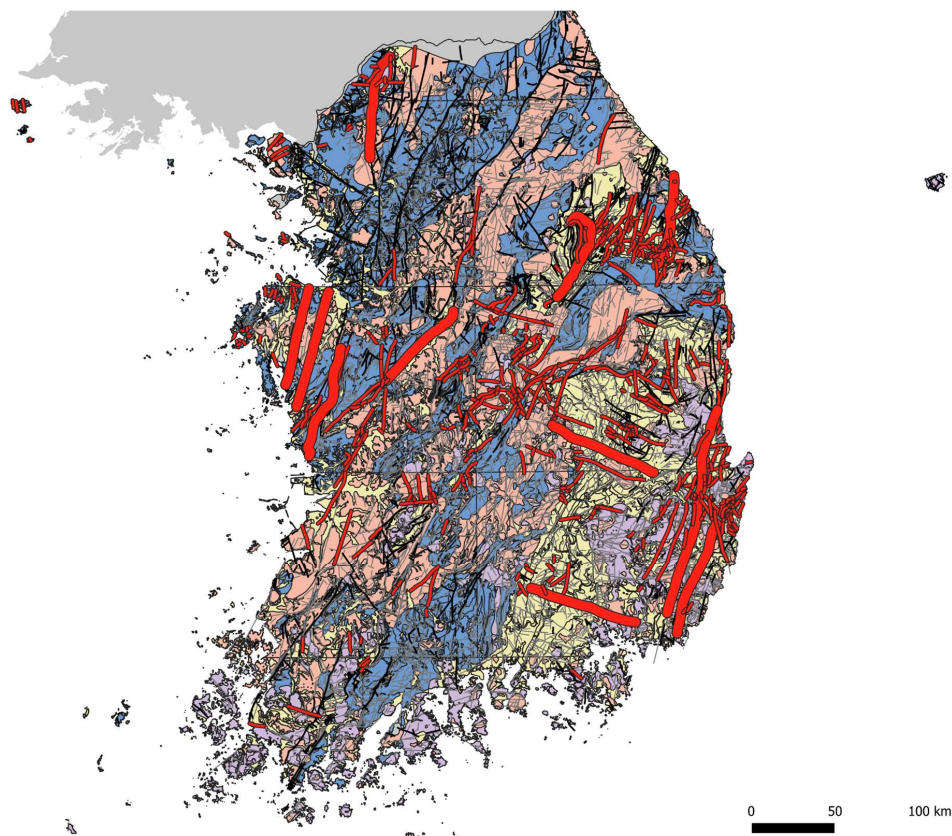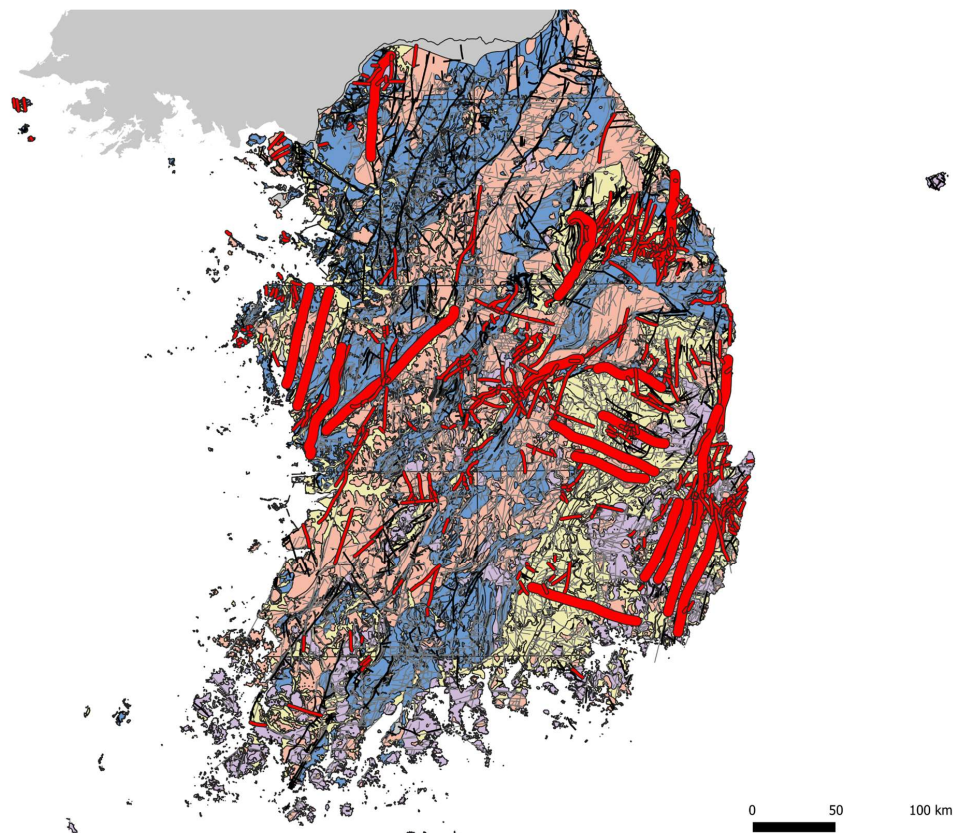
725 **Figure A7. Potentially active regional and supra-regional fault zones in South-Korea buffered by a 1-km- and a 3-km-safety buffer (red polygons), respectively, according to the German approach. Here, we distinguish supra-regional fault zones by length (>50 km) from regional faults zones (<50 km). For dataset description see table A11.**

Table A7. Areal statistics of the areas covered by the 1-km- and 3-km-buffer drawn around faults that touch or intersect an earthquake cluster in each of the rock types in the geological map of South-Korea. The entire 1-km- and 3-km-buffer area covers
730 **12.23 % of the onshore portion of South-Korea, i.e. adding 2.93 % to the 1-km-buffer area.**

Rock Types (aggregated)	Area km²	Area %	Faults In EQ-clusters 1&3km-buffer-area (50 km Limit)		
	km²	%	m²	km²	%
Granites	29,095	29	2,798,400,446	2,798	10
Deformed Rocks (incl. schist and gneiss)	28,458	29	2,412,583,849	2,413	8

46

|					
Sedimentary Rocks	28,891	29	5,847,938,881	5,848	20
Igneous Rocks	12,987	13	1,096,901,815	1,097	8
Sum	**99,431**	**100**	**12,155,824,990**	**12,156**	**12.23**

Figure A8. Potentially active regional and supra-regional fault zones in South-Korea buffered by a 1-km- and a 3-km-safety buffer (red polygons), respectively, according to the German approach. Here, we distinguish supra-regional fault zones by length (>40 km) from regional faults zones (<40 km). For dataset description see table A11.

Table A8. Areal statistics of the areas covered by the 1-km- and 3-km-buffer drawn around faults that touch or intersect an earthquake cluster in each of the rock types in the geological map of South-Korea. The entire 1-km- and 3-km-buffer area covers 13.57 % of the onshore portion of South-Korea, i.e. adding 4.28 % to the 1-km-buffer area.

47

| Rock Types (aggregated)	Area km^2	Area %	Faults In EQ-clusters 1&3km-buffer-area (40 km Limit)		
	km^2	%	m^2	km^2	%
Granites	29,095	29	3,190,804,116	3,191	11
Deformed Rocks (incl. schist and gneiss)	28,458	29	2,545,854,086	2,546	9
Sedimentary Rocks	28,891	29	6,333,500,607	6,334	22
Igneous Rocks	12,987	13	1,424,887,525	1,425	11
Sum	**99,431**	**100**	**13,495,046,334**	**13,495**	**13.57**
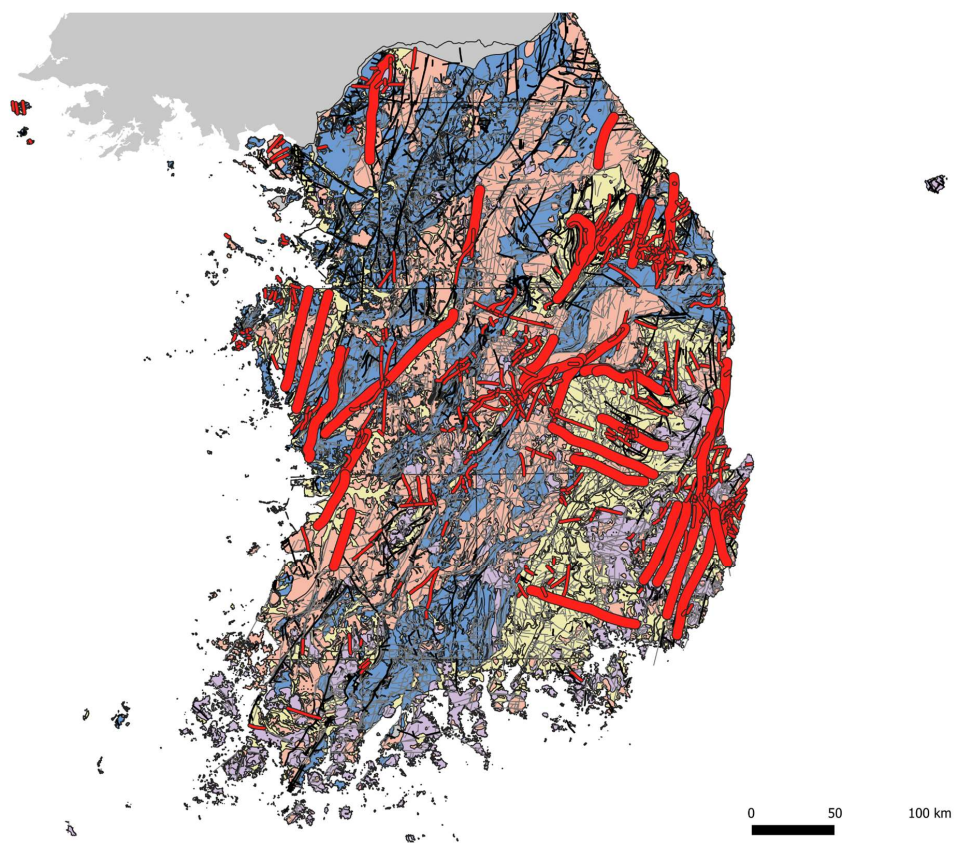
740

Figure A9. Potentially active regional and supra-regional fault zones in South-Korea buffered by a 1-km- and a 3-km-safety buffer (red polygons), respectively, according to the German approach. Here, we distinguish supra-regional fault zones by length (>30 km) from regional faults zones (<30 km). For dataset description see table A11.

745 **Table A9. Areal statistics of the areas covered by the 1-km- and 3-km-buffer drawn around faults that touch or intersect an earthquake cluster in each of the rock types in the geological map of South-Korea. The entire 1-km- and 3-km-buffer area covers 15.12 % of the onshore portion of South-Korea, i.e. adding 5.82 % to the 1-km-buffer area.**

Rock Types (aggregated)	Area km²	Area %	Faults In EQ-clusters 1&3km-buffer_area(30kmLimit)		
	km²	%	m²	km²	%
Granites	29,095	29	3,858,351,710	3,858	13
Deformed Rocks (incl. schist and gneiss)	28,458	29	2,777,950,495	2,778	10
Sedimentary Rocks	28,891	29	6,941,550,143	6,942	24
Igneous Rocks	12,987	13	1,452,036,857	1,452	11
Sum	**99,431**	**100**	**15,029,889,205**	**15,030**	**15.12**
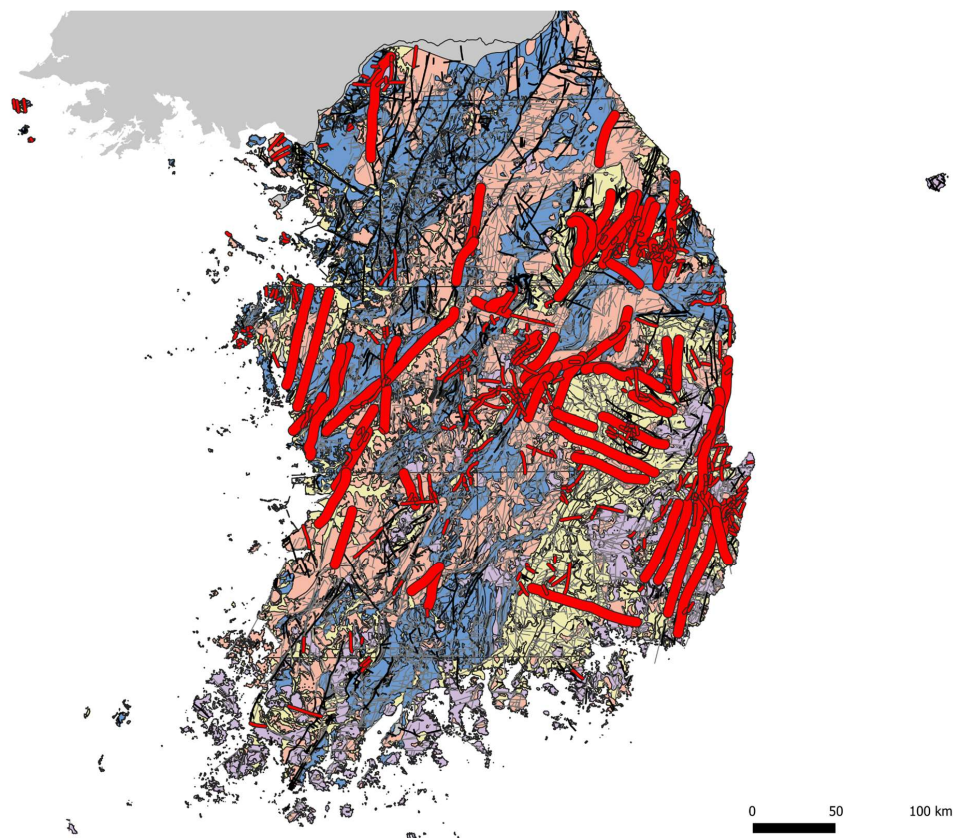
Figure A10. Potentially active regional and supra-regional fault zones in South-Korea buffered by a 1-km- and a 3-km-safety buffer
750 **(red polygons), respectively, according to the German approach. Here, we distinguish supra-regional fault zones by length (>20 km) from regional faults zones (<20 km). For dataset description see table A11.**

Table A10. Areal statistics of the areas covered by the 1-km- and 3-km-buffer drawn around faults that touch or intersect an earthquake cluster in each of the rock types in the geological map of South-Korea. The entire 1-km- and 3-km-buffer area covers 17.22 % of the onshore portion of South-Korea, i.e. adding 7.93 % to the 1-km-buffer area.

Rock Types (aggregated)	Area km²	Area %	Faults In EQ-clusters 1&3km-buffer_area(10kmLimit)		
	km²	%	m²	km²	%
Granites	29,095	29	4,453,761,180	4,454	15
Deformed Rocks (incl. schist and gneiss)	28,458	29	3,389,886,656	3,390	12
Sedimentary Rocks	28,891	29	7,778,927,808	7,779	27
Igneous Rocks	12,987	13	1,502,145,441	1,502	12

Sum	**99,431**	**100**	**17,124,721,085**	**17,125**	**17.22**

755

Table A11. List of shapefiles and raster images provided as online supplementary material. Datasets are briefly described.

Type of Dataset	Geospatial Dataset (filename, file size)	Dataset Description
1)	*Geological map (Rock Type polygons, faults and lineaments):*	
Polygons:	Data_20230512 — ROCk.cpg , 5 KB Data_20230512 — ROCk.dbf , 3387426 KB Data_20230512 — ROCk.gpkg , 13156352 KB Data_20230512 — ROCk.prj , 420 KB Data_20230512 — ROCk.shp , 9881304 KB Data_20230512 — ROCk.shx , 73732 KB	Areas of 11 Rock Types in 246 Rock Units of South-Korea. Geological map served as basis for simplified map used in this work.
Polygons:	Data_20230512 — ROCk (byRockTY_aggregated)_Collected.cpg , 5 KB Data_20230512 — ROCk (byRockTY_aggregated)_Collected.dbf , 4687 KB Data_20230512 — ROCk (byRockTY_aggregated)_Collected.gpkg, 9613312 KB Data_20230512 — ROCk (byRockTY_aggregated)_Collected.prj , 420 KB Data_20230512 — ROCk (byRockTY_aggregated)_Collected.shp , 9403268 KB Data_20230512 — ROCk (byRockTY_aggregated)_Collected.shx , 188 KB	Areas of 11 Rock Types collected in 4 groups: 1.) granites, 2.) metamorphic rocks, 3.) sedimentary rocks, and 4.) igneous rocks (simplified geological map, as used in this work).
Line segments:	Data_20230512 — fault (n=1528).cpg , 5 KB Data_20230512 — fault (n=1528).dbf , 718642 KB Data_20230512 — fault (n=1528).gpkg , 1191936 KB Data_20230512 — fault (n=1528).prj , 420 KB Data_20230512 — fault (n=1528).shp , 728528 KB Data_20230512 — fault (n=1528).shx , 12324 KB	Surface traces of Faults in South-Korea. Displayed as black lines in Figures.
Line segments:	Data_20230512 — Lineament (n=6654).cpg , 5 KB Data_20230512 — Lineament (n=6654).dbf , 392748 KB Data_20230512 — Lineament (n=6654).gpkg , 1646592 KB Data_20230512 — Lineament (n=6654).prj , 420 KB Data_20230512 — Lineament (n=6654).shp , 895504 KB Data_20230512 — Lineament (n=6654).shx , 53332 KB	Lineament traces of South-Korea. Displayed as grey lines in Figures.
2)	*EQ-catalogue, Heatmap 1 and resulting EQ-clusters:*	
Point cloud:	KoreaEQ_1991-01-01_2023-05-10.gpkg , 6627328 KB	Point cloud of epicenter locations in the Earthquake catalogue (red filled circles in Fig. 4).
Raster image:	KoreaEQ_HeatmapKDE_Radius0.1degPxSize0.01.tif , 507530 KB	10-km-kernel Heatmap raster image of epicenter locations (Kernel Radius: 0.1 deg, Pixel Size: 0.01 deg) for

		earthquake cluster analysis (Fig. 5, Fig. 6).
Contour line:	KoreaEQ_HeatmapKDE_Radius0.1degPxSize0.01_contoursInterval1.cpg , 5 KB KoreaEQ_HeatmapKDE_Radius0.1degPxSize0.01_contoursInterval1.dbf , 25970 KB KoreaEQ_HeatmapKDE_Radius0.1degPxSize0.01_contoursInterval1.prj , 145KB KoreaEQ_HeatmapKDE_Radius0.1degPxSize0.01_contoursInterval1.shp , 327924 KB KoreaEQ_HeatmapKDE_Radius0.1degPxSize0.01_contoursInterval1.shx , 6372 KB KoreaEQ_HeatmapKDE-Rad0.1_Level-1-contour_geometry.cpg , 5 KB KoreaEQ_HeatmapKDE-Rad0.1_Level-1-contour_geometry.dbf , 44818 KB KoreaEQ_HeatmapKDE-Rad0.1_Level-1-contour_geometry.prj , 145 KB KoreaEQ_HeatmapKDE-Rad0.1_Level-1-contour_geometry.shp , 327924 KB KoreaEQ_HeatmapKDE-Rad0.1_Level-1-contour_geometry.shx , 6372 KB	Level 1 Heatmap contour lines of epicenter locations in earthquake catalogue.
Polygons:	KoreaEQ_HeatmapKDE-Rad0.1contour_geometry_polygons_geometry_outerbound.cpg , 5 KB KoreaEQ_HeatmapKDE-Rad0.1contour_geometry_polygons_geometry_outerbound.dbf , 21383 KB KoreaEQ_HeatmapKDE-Rad0.1contour_geometry_polygons_geometry_outerbound.prj , 145 KB KoreaEQ_HeatmapKDE-Rad0.1contour_geometry_polygons_geometry_outerbound.shp , 99100 KB KoreaEQ_HeatmapKDE-Rad0.1contour_geometry_polygons_geometry_outerbound.shx , 1452 KB	Outlines of Onshore and offshore Earthquake clusters (purple areas in Fig. 7, Fig. A4, Fig. A6).
Polygons:	KoreaEQ_HeatmapKDE-Rad0.1contour_geometry_polygons_geometry_outerbound_mainland.cpg , 5 KB KoreaEQ_HeatmapKDE-Rad0.1contour_geometry_polygons_geometry_outerbound_mainland.dbf , 17780 KB KoreaEQ_HeatmapKDE-Rad0.1contour_geometry_polygons_geometry_outerbound_mainland.prj , 145 KB KoreaEQ_HeatmapKDE-Rad0.1contour_geometry_polygons_geometry_outerbound_mainland.shp , 591456 KB KoreaEQ_HeatmapKDE-Rad0.1contour_geometry_polygons_geometry_outerbound_mainland.shx , 724 KB	Outlines of Onshore Earthquake clusters (violet areas in Fig. 7, Fig. A4, Fig. A6).
3)	*Faults intersecting/touching EQ-clusters:*	
Line segments:	FaultsInEQclusters0.1contour (n=457).cpg , 5 KB FaultsInEQclusters0.1contour (n=457).dbf , 191476 KB FaultsInEQclusters0.1contour (n=457).prj , 145 KB FaultsInEQclusters0.1contour (n=457).shp , 257804 KB FaultsInEQclusters0.1contour (n=457).shx , 3756 KB	Surface traces of faults which intersect or touch earthquake clusters. Displayed as red lines in Fig.7 and Fig. A4.
Line segments:	FaultsOutsideEQclusters (n=1077).cpg , 5 KB FaultsOutsideEQclusters (n=1077).dbf , 380471 KB FaultsOutsideEQclusters (n=1077).prj , 420 KB FaultsOutsideEQclusters (n=1077).shp , 471912 KB	Surface traces of faults which do not intersect or touch earthquake clusters

	FaultsOutsideEQclusters (n=1077).shx , 8716 KB	
4)	***Heatmap 2 and resulting EQ-epicenter search kernels:***	
Raster image:	KoreaEQ_HeatmapKDE_Radius0.01degPxSize0.01.tif , 3028314 KB	2x2-km-kernel Heatmap raster image of epicenter locations in earthquake catalogue (Kernel Radius: 0.01deg, Pixel Size: 0.01deg) for colocation of faults and epicenters
Polygons:	KoreaEQ_HeatmapKDE_Radius0.01degPxSize0.01_ Polygons_geometry.cpg , 5 KB KoreaEQ_HeatmapKDE_Radius0.01degPxSize0.01_ Polygons_geometry.dbf , 14676 KB KoreaEQ_HeatmapKDE_Radius0.01degPxSize0.01_ Polygons_geometry.prj , 145 KB KoreaEQ_HeatmapKDE_Radius0.01degPxSize0.01_ Polygons_geometry.shp , 205044 KB KoreaEQ_HeatmapKDE_Radius0.01degPxSize0.01_ Polygons_geometry.shx , 11788 KB	Outlines of the 2x2-km-kernels onshore and offshore Korea (red filled areas in Fig. A3)
Polygons:	KoreaEQ_HeatmapKDE_Radius 0.01degPxSize0.01_Polygons_geometry_mainland.cpg , 5 KB KoreaEQ_HeatmapKDE_Radius 0.01degPxSize0.01_Polygons_geometry_mainland.dbf , 17780 KB KoreaEQ_HeatmapKDE_Radius 0.01degPxSize0.01_Polygons_geometry_mainland.prj , 145 KB KoreaEQ_HeatmapKDE_Radius 0.01degPxSize0.01_Polygons_geometry_mainland.shp , 591456 KB KoreaEQ_HeatmapKDE_Radius 0.01degPxSize0.01_Polygons_geometry_mainland.shx , 724 KB	Outlines of the 2x2-km-kernels onshore Korea.
5)	***Faults within 1 km range of EQ-epicenters:***	
Line segments:	FaultsOnEpicenters_Rad0.01degPxSize0.01deg (n=163).cpg , 5 KB FaultsOnEpicenters_Rad0.01degPxSize0.01deg (n=163).dbf , 64739 KB FaultsOnEpicenters_Rad0.01degPxSize0.01deg (n=163).prj , 420 KB FaultsOnEpicenters_Rad0.01degPxSize0.01deg (n=163).shp , 75860 KB FaultsOnEpicenters_Rad0.01degPxSize0.01deg (n=163).shx , 1404 KB	Surface traces of fault zones within 1 km range of earthquake epicenters (yellow lines in Fig. 7 and Fig. A4).
6)	***Faults and lineaments coloured by rock type***	
Line segments:	Data_20230512-fault_intersectwith_Rock(byRockTY_aggregated)_Collected_fgeo.cpg , 5 KB Data_20230512-fault_intersectwith_Rock(byRockTY_aggregated)_Collected_fgeo.dbf , 4183845 KB Data_20230512-fault_intersectwith_Rock(byRockTY_aggregated)_Collected_fgeo.prj , 420 KB Data_20230512-fault_intersectwith_Rock(byRockTY_aggregated)_Collected_fgeo.shp , 935696 KB Data_20230512-fault_intersectwith_Rock(byRockTY_aggregated)_Collected_fgeo.shx , 26764 KB	Surface traces of fault zones intersected with Rock Type (displayed as lines coloured by Rock Type in Fig. 3).

Line segments:	Data_20230512-lineament_intersectwith_Rock(byRockTY_aggregated)_Collected_fgeo.cpg , 5 KB Data_20230512-lineament_intersectwith_Rock(byRockTY_aggregated)_Collected_fgeo.dbf , 9765307 KB Data_20230512-lineament_intersectwith_Rock(byRockTY_aggregated)_Collected_fgeo.prj , 420 KB Data_20230512-lineament_intersectwith_Rock(byRockTY_aggregated)_Collected_fgeo.shp , 1632180 KB Data_20230512-lineament_intersectwith_Rock(byRockTY_aggregated)_Collected_fgeo.shx , 99868 KB	Line segments of lineaments intersected with Rock Type (displayed as lines coloured by Rock Type in Fig. 3).
7)	*Potentially active fault zones (combining results from 3) and 5)):*	
Line segments:	FaultsInEQclusters0.1contour_FaultsOnEpicenters_merged_uniques (n=488).cpg , 5 KB FaultsInEQclusters0.1contour_FaultsOnEpicenters_merged_uniques (n=488).dbf , 462682 KB FaultsInEQclusters0.1contour_FaultsOnEpicenters_merged_uniques (n=488).gpkg , 3072000 KB FaultsInEQclusters0.1contour_FaultsOnEpicenters_merged_uniques (n=488).prj , 420 KB FaultsInEQclusters0.1contour_FaultsOnEpicenters_merged_uniques (n=488).shp , 270164 KB FaultsInEQclusters0.1contour_FaultsOnEpicenters_merged_uniques (n=488).shx , 4004KB	Surface traces of fault zones in both earthquake clusters and within 1 km range of an epicenter location. Displayed as red lines in Fig. A6.
Line segments:	FaultsInEQclusters0.1contour _FaultsOnEpicenters_merged_uniques (n=488)_intersectWith_Rock(byRockTy_aggregated)_Collected_fgeo.cpg , 5 KB FaultsInEQclusters0.1contour_FaultsOnEpicenters_merged_uniques (n=488)_intersectWith_Rock(byRockTy_aggregated)_Collected_fgeo.dbf , 1939123 KB FaultsInEQclusters0.1contour_FaultsOnEpicenters_merged_uniques (n=488)_intersectWith_Rock(byRockTy_aggregated)_Collected_fgeo.prj , 420 KB FaultsInEQclusters0.1contour_FaultsOnEpicenters_merged_uniques (n=488)_intersectWith_Rock(byRockTy_aggregated)_Collected_fgeo.shp , 351268 KB FaultsInEQclusters0.1contour_FaultsOnEpicenters_merged_uniques (n=488)_intersectWith_Rock(byRockTy_aggregated)_Collected_fgeo.shx , 9324 KB	Surface traces of fault zones in both, earthquake clusters and within 1 km range of an epicenter location intersected with Rock Type. Displayed as coloured lines in Fig. 9.
8)	*Japan-style buffer areas:*	
Polygons:	FaultsInEQclusters0.1contour _FaultsOnEpicenters_merged_Ldiv100-buffer.cpg , 5 KB FaultsInEQclusters0.1contour _FaultsOnEpicenters_merged_Ldiv100-buffer.dbf , 462682 KB FaultsInEQclusters0.1contour _FaultsOnEpicenters_merged_Ldiv100-buffer.gpkg , 1249280 KB	Outlines of Length/100 buffer areas around potentially active fault zones (red areas in Fig. 13).

	FaultsInEQclusters0.1contour _FaultsOnEpicenters_merged_Ldiv100-buffer.prj , 420 KB	
	FaultsInEQclusters0.1contour _FaultsOnEpicenters_merged_Ldiv100-buffer.shp , 825416 KB	
	FaultsInEQclusters0.1contour _FaultsOnEpicenters_merged_Ldiv100-buffer.shx , 4004 KB	
Polygons:	FaultsInEQclusters0.1contour _FaultsOnEpicenters_merged_Ldiv50-buffer.cpg , 5 KB	Outlines of Length/50 buffer areas around potentially active fault zones (red areas in Fig. 14).
	FaultsInEQclusters0.1contour _FaultsOnEpicenters_merged_Ldiv50-buffer.dbf , 462682 KB	
	FaultsInEQclusters0.1contour _FaultsOnEpicenters_merged_Ldiv50-buffer.gpkg , 1236992 KB	
	FaultsInEQclusters0.1contour _FaultsOnEpicenters_merged_Ldiv50-buffer.prj , 420 KB	
	FaultsInEQclusters0.1contour _FaultsOnEpicenters_merged_Ldiv50-buffer.shp , 817124 KB	
	FaultsInEQclusters0.1contour _FaultsOnEpicenters_merged_Ldiv50-buffer.shx , 4004 KB	
9)	*Swedish-style buffers (100m,50m,5m respect distances applied to all faults of 10-130 km, 1-10 km, and 0-1 km length, respectively):*	
Polygons:	Data_20230512-fault(n=1528)_100m,50m,5m-buffer(10-130km,1-10km,0-1km)_03.cpg , 5 KB	Outlines of 100-m-, 50-m-, and 5-m-buffer areas for 10-130km, 1-10km, and 0-1km length fault zones (red areas in Fig. 15).
	Data_20230512-fault(n=1528)_100m,50m,5m-buffer(10-130km,1-10km,0-1km)_03.dbf , 796634 KB	
	Data_20230512-fault(n=1528)_100m,50m,5m-buffer(10-130km,1-10km,0-1km)_03.prj , 420 KB	
	Data_20230512-fault(n=1528)_100m,50m,5m-buffer(10-130km,1-10km,0-1km)_03.shp , 2275428 KB	
	Data_20230512-fault(n=1528)_100m,50m,5m-buffer(10-130km,1-10km,0-1km)_03.shx , 12324 KB	
10)	*German-style buffer areas:*	
Polygons:	FaultsInEQclusters0.1contour_FaultsOnEpicenters_merged_1km-buffer.cpg , 5 KB	Outlines of 1-km buffer areas around potentially active fault zones (red areas in Fig. 17).
	FaultsInEQclusters0.1contour_FaultsOnEpicenters_merged_1km-buffer.dbf , 462682 KB	
	FaultsInEQclusters0.1contour_FaultsOnEpicenters_merged_1km-buffer.gpkg , 1171456 KB	
	FaultsInEQclusters0.1contour_FaultsOnEpicenters_merged_1km-buffer.prj , 420 KB	
	FaultsInEQclusters0.1contour_FaultsOnEpicenters_merged_1km-buffer.shp , 745576 KB	
	FaultsInEQclusters0.1contour_FaultsOnEpicenters_merged_1km-buffer.shx , 4004 KB	
Polygons:	FaultsInEQclusters0.1contour_FaultsOnEpicenters_merged_1&3km-buffer(10kmLimit).cpg , 5 KB	Outlines of 1-km and 3-km buffer areas around potentially active fault zones distinguishing zones <10km and >10km (red areas in Fig. 18).
	FaultsInEQclusters0.1contour_FaultsOnEpicenters_merged_1&3km-buffer(10kmLimit).dbf , 462682 KB	
	FaultsInEQclusters0.1contour_FaultsOnEpicenters_merged_1&3km-buffer(10kmLimit).gpkg , 1105920 KB	

	FaultsInEQclusters0.1contour_FaultsOnEpicenters_merged_1&3km-buffer(10kmLimit).prj , 420 KB FaultsInEQclusters0.1contour_FaultsOnEpicenters_merged_1&3km-buffer(10kmLimit).shp , 713932 KB FaultsInEQclusters0.1contour_FaultsOnEpicenters_merged_1&3km-buffer(10kmLimit).shx , 4004 KB	
Polygons:	FaultsInEQclusters0.1contour_FaultsOnEpicenters_merged_1&3km-buffer(50kmLimit).cpg , 5 KB FaultsInEQclusters0.1contour_FaultsOnEpicenters_merged_1&3km-buffer(50kmLimit).dbf , 462682 KB FaultsInEQclusters0.1contour_FaultsOnEpicenters_merged_1&3km-buffer(50kmLimit).gpkg , 1167360 KB FaultsInEQclusters0.1contour_FaultsOnEpicenters_merged_1&3km-buffer(50kmLimit).prj , 420 KB FaultsInEQclusters0.1contour_FaultsOnEpicenters_merged_1&3km-buffer(50kmLimit).shp , 741868 KB FaultsInEQclusters0.1contour_FaultsOnEpicenters_merged_1&3km-buffer(50kmLimit).shx , 4004 KB	Outlines of 1-km and 3-km buffer areas around potentially active fault zones distinguishing zones <50km and >50km (red areas in Fig. A7).
Polygons:	FaultsInEQclusters0.1contour_FaultsOnEpicenters_merged_1&3km-buffer(40kmLimit).cpg , 5 KB FaultsInEQclusters0.1contour_FaultsOnEpicenters_merged_1&3km-buffer(40kmLimit).dbf , 462682 KB FaultsInEQclusters0.1contour_FaultsOnEpicenters_merged_1&3km-buffer(40kmLimit).gpkg , 1163264 KB FaultsInEQclusters0.1contour_FaultsOnEpicenters_merged_1&3km-buffer(40kmLimit).prj , 420 KB FaultsInEQclusters0.1contour_FaultsOnEpicenters_merged_1&3km-buffer(40kmLimit).shp , 741484 KB FaultsInEQclusters0.1contour_FaultsOnEpicenters_merged_1&3km-buffer(40kmLimit).shx , 4004 KB	Outlines of 1-km and 3-km buffer areas around potentially active fault zones distinguishing zones <40km and >40km (red areas in Fig. A8).
Polygons:	FaultsInEQclusters0.1contour_FaultsOnEpicenters_merged_1&3km-buffer(30kmLimit).cpg , 5 KB FaultsInEQclusters0.1contour_FaultsOnEpicenters_merged_1&3km-buffer(30kmLimit).dbf , 462682 KB FaultsInEQclusters0.1contour_FaultsOnEpicenters_merged_1&3km-buffer(30kmLimit).gpkg , 1155072 KB FaultsInEQclusters0.1contour_FaultsOnEpicenters_merged_1&3km-buffer(30kmLimit).prj , 420 KB FaultsInEQclusters0.1contour_FaultsOnEpicenters_merged_1&3km-buffer(30kmLimit).shp , 732764 KB FaultsInEQclusters0.1contour_FaultsOnEpicenters_merged_1&3km-buffer(30kmLimit).shx , 4004 KB	Outlines of 1-km and 3-km buffer areas around potentially active fault zones distinguishing zones <30km and >30km (red areas in Fig. A9).
Polygons:	FaultsInEQclusters0.1contour_FaultsOnEpicenters_merged_1&3km-buffer(20kmLimit).cpg , 5 KB FaultsInEQclusters0.1contour_FaultsOnEpicenters_merged_1&3km-buffer(20kmLimit).dbf , 462682 KB FaultsInEQclusters0.1contour_FaultsOnEpicenters_merged_1&3km-buffer(20kmLimit).gpkg , 1134592 KB FaultsInEQclusters0.1contour_FaultsOnEpicenters_merged_1&3km-buffer(20kmLimit).prj , 420 KB	Outlines of 1-km and 3-km buffer areas around potentially active fault zones distinguishing zones <20km and >20km (red areas in Fig. A10).

	FaultsInEQclusters0.1contour _FaultsOnEpicenters_merged_1&3km-buffer(20kmLimit).shp , 728764 KB FaultsInEQclusters0.1contour _FaultsOnEpicenters_merged_1&3km-buffer(20kmLimit).shx , 4004 KB	

760 **FaultsInEQclusters0.1contourFaultsInEQclusters0.1contourFaultsInEQclusters0.1contourFaultsInEQclusters0.1contourFaultsInEQclusters0.1contourFaultsInEQclusters0.1contourFaultsInEQclusters0.1contourFaultsInEQclusters0.1contourFaultsInEQclusters0.1contourFaultsInEQclusters0.1contourFaultsInEQclusters0.1contourFaultsInEQclusters0.1contourReferences**

Barnett, J.A., Mortimer, J., Rippon, J.H., Walsh, J.J. and Watterson, J., (1987). Displacement geometry in the volume containing a single normal fault. *AAPG bulletin*, *71*(8), pp.925-937. DOI: 10.1306/948878ED-1704-11D7-8645000102C1865D

765 Båth, Markus (1978). The seismicity of Sweden, Geologiska Föreningen i Stockholm Förhandlingar, 100:3, 295-299, DOI: 10.1080/11035897809452539

BGE (2020). Sub-areas Interim Report pursuant to Section 13 StandAG. Peine: Bundesgesellschaft für Endlagerung mbH. As per 28/09/2020. https://www.bge.de/fileadmin/user_upload/Standortsuche/Wesentliche_Unterlagen/Zwischenbericht_Teilgebiete/Zwischenb

770 ericht_Teilgebiete_-_Englische_Fassung_barrierefrei.pdf

BGE (2022). Methodenbeschreibung zur Durchführung der repräsentativen vorläufigen Sicherheitsuntersuchungen gemäß Endlagersicherheitsuntersuchungsverordnung. Stand 28.03.2022. Geschäftszeichen: SG02303/97-2/2-2022#10 – Objekt-ID: 919256 – Revision: 00. https://www.bge.de/fileadmin/user_upload/Standortsuche/Wesentliche_Unterlagen/Methodik/Phase_I_Schritt_2/rvSU-

775 Methodik/20220328_Anlage_zu_rvSU_Konzept_Methodenbeschreibung_barrierefrei.pdf

Bilgilioğlu, S.S., (2022). Site selection for radioactive waste disposal facility by GIS based multi criteria decision making. *Annals of Nuclear Energy*, *165*, p.108795. DOI: 10.1016/j.anucene.2021.108795

BT-Drs.18-11398 (2017). Bundestag-Drucksache 18/11398, Gesetzentwurf Standortauswahlgesetz – StandAG, 07.03.2017. https://dserver.bundestag.de/btd/18/113/1811398.pdf

780 Byerlee, J.D. (1967). Frictional characteristics of granite under high confining pressure. *Journal of Geophysical Research*, *72*(14), pp.3639-3648. DOI: 10.1029/JZ072i014p03639

Calais, E., Camelbeeck, T., Stein, S., Liu, M. and Craig, T.J., (2016). A new paradigm for large earthquakes in stable continental plate interiors. Geophysical Research Letters, 43(20), pp.10-621. DOI: 10.1002/2016GL070815

Cappa, F. and Rutqvist, J., (2011). Modeling of coupled deformation and permeability evolution during fault reactivation

785 induced by deep underground injection of CO_2. International Journal of Greenhouse Gas Control, 5(2), pp.336-346. https://doi.org/10.1016/j.ijggc.2010.08.005

Chen, Y.C., 2017. A tutorial on kernel density estimation and recent advances. Biostatistics & Epidemiology, 1(1), pp.161-187. https://doi.org/10.1080/24709360.2017.1396742

Choi, Heui-Joo, Jong Youl Lee, Dong-Keun Cho, Sungki Kim, Seungsu Kim, Gunyoung Kim, Jongtae Jeong, Minsoo Lee,
790   Jongwon Choi (2008). "Korean Reference HLW Disposal System," KAERI/TR-3653/2008, KAERI (2008). https://www.osti.gov/etdeweb/biblio/21200013

Choi, Heui-Joo, Minsoo Lee, Jong Youl Lee (2011). Preliminary conceptual design of a geological disposal system for high-level wastes from the pyroprocessing of PWR spent fuels. Nuclear Engineering and Design 241 (2011) 3348– 3356. doi:10.1016/j.nucengdes.2011.06.013

795   Choi, H.J., Lee, J.Y. and Choi, J., (2013). Development of geological disposal systems for spent fuels and high-level radioactive wastes in Korea. Nuclear Engineering and Technology, 45(1), pp.29-40. DOI: 10.5516/NET.06.2012.006

Choi, Sung-Ja; Jeon, Jeong Soo; Choi, Jeong-Heon; Kim, Bokchul; Ryoo, Chung-Ryul; Hong, Duk-Geun; Chwae, Ueechan (2014). Estimation of possible maximum earthquake magnitudes of Quaternary faults in the southern Korean Peninsula. Quaternary International, 344(), 53–63. doi:10.1016/j.quaint.2014.05.052

800   De Jong, K., Han, S. and Ruffet, G. (2015). Fast cooling following a Late Triassic metamorphic and magmatic pulse: implications for the tectonic evolution of the Korean collision belt. Tectonophysics, 662, pp.271-290. https://doi.org/10.1016/j.tecto.2015.06.016

Galadini, F., Falcucci, E., Galli, P., Giaccio, B., Gori, S., Messina, P., Moro, M., Saroli, M., Scardia, G. and Sposato, A. (2012). Time intervals to assess active and capable faults for engineering practices in Italy. Engineering geology, 139, pp.50-65.
805   https://doi.org/10.1016/j.enggeo.2012.03.012

Global Administrative Areas (Version 4.1, released on 16 July 2022). University of California, Berkely. [digital geospatial data: gadm40_KOR_0.shp, gadm40_PRK_0.shp]. Available online: http://www.gadm.org [14/07/2023].

Ha, S., Son, M. and Seong, Y.B. (2022). Active fault trace identification using a LiDAR high-resolution DEM: A case study of the central Yangsan Fault, Korea. *Remote Sensing*, *14*(19), p.4838. https://www.mdpi.com/2072-4292/14/19/4838/pdf

810   Han, M., Kim, K.H., Son, M. and Kang, S.Y. (2017). Current microseismicity and generating faults in the Gyeongju area, southeastern Korea. Tectonophysics, 694, pp.414-423. https://www.sciencedirect.com/science/article/abs/pii/S0040195116305443

He, X., Xu, C., Xu, X. and Yang, Y. (2022). Advances on the avoidance zone and buffer zone of active faults. Natural Hazards Research, 2(2), pp.62-74. https://doi.org/10.1016/j.nhres.2022.05.001

815   Houng, S. E.; Hong, T.-K. (2013). *Probabilistic Analysis of the Korean Historical Earthquake Records. Bulletin of the Seismological Society of America, 103(5), 2782–2796.* doi:10.1785/0120120318

Jin, Shuanggen and Pil-Ho Park (2006). Crustal Stress and Strain Energy Density Rates in South Korea Deduced from GPS Observations. TAO, Vol. 17, No. 1, March 2006

KIGAM (2019). Korea Geological Resources Research report of 2019. Korea Institute of Geoscience and Mineral Resources,
820   2020-04-10. https://www.kigam.re.kr/

Kim, Chun-soo, Dae-seok Bae, Kyung-su Kim, Byung-yun Park, Young-kown Koh, Kwan-sik Jeon, and Jinwoong Kim (2000). A preliminary study on the suitability of host rocks for deep geological disposal of high level radioactive waste in Korea. KAERI/TR-1521/2000, 140p

Kim, T. and Park, H. (2017). Perceptional differences in the factors of local acceptance of spent nuclear fuel repositories. Land
825   Use Policy, 67, pp.702-709. DOI: 10.1016/j.landusepol.2017.07.011

Kim, Young-Seog, Moon Son, Jin-Hyuck Choi, Jeong-Heon Choi, Yeong Bae Seong and Jinhyun Lee, (2020). Processes and challenges for the production of Korean active faults map. Journal of the Geological Society of Korea. v. 56, no. 2, p. 113-134, (April 2020). DOI http://dx.doi.org/10.14770/jgsk.2020.56.2.113

Kim, T., Choi, J.H., Cheon, Y., Lee, T.H., Kim, N., Lee, H., Kim, C.M., Choi, Y., Bae, H., Kim, Y.S. and Ryoo, C.R. (2023).
830   Correlation of paleoearthquake records at multiple sites along the southern Yangsan Fault, Korea: Insights into rupture scenarios of intraplate strike-slip earthquakes. Tectonophysics, 854, p.229817. https://doi.org/10.1016/j.tecto.2023.229817

Kim, N., Park, S.I., Cho, C.S., Cheon, Y. and Peace, A.L. (2023). Neotectonic transpressional intraplate deformation in eastern Eurasia: Insights from active fault systems in the southeastern Korean Peninsula. Geoscience Frontiers, 14(4), p.101559. https://doi.org/10.1016/j.gsf.2023.101559

835   Kwon, Sanghoon, K. Sajeev, Gautam Mitra, Youngdo Park, Sung Won Kim, In-Chang Ryu (2009). Evidence for Permo-Triassic collision in Far East Asia: The Korean collisional orogen. Earth and Planetary Science Letters 279 (2009) 340–349. https://doi.org/10.1016/j.epsl.2009.01.016

Lee, K., Chung, N.S. and Chung, T.W. (2003). Earthquakes in Korea from 1905 to 1945. *Bulletin of the Seismological Society of America*, *93*(5), pp.2131-2145. https://doi.org/10.1785/0120020176

840   Lee, Kiehwa and Woo-Sun Yang (2006). Historical Seismicity of Korea. Bulletin of the Seismological Society of America (2006) 96 (3): 846–855. https://doi.org/10.1785/0120050050

Lee, Jongyoul, Dongkeun Cho , Heuijoo Choi & Jongwon Choi (2007). Concept of a Korean Reference Disposal System for Spent Fuels, Journal of Nuclear Science and Technology, 44:12, 1565-1573, DOI: 10.1080/18811248.2007.9711407

Mays, G.T., Belles, R., Blevins, B.R., Hadley, S.W., Harrison, T.J., Jochem, W.C., Neish, B.S., Omitaomu, O.A. and Rose,
845   A.N., 2012. Application of spatial data modeling and geographical information systems (GIS) for identification of potential siting options for various electrical generation sources. ORNL/TM-2011/157, 1. https://info.ornl.gov/sites/publications/files/Pub30613.pdf

Moeck, I., Kwiatek, G., Zimmermann, G. (2009). Slip tendency analysis, fault reactivation potential and induced seismicity in a deep geothermal reservoir. Journal of Structural Geology. 2009 Oct 1;31(10):1174-82.
850   https://doi.org/10.1016/j.jsg.2009.06.012

Mogi, K. (1981). Seismicity in western Japan and long-term earthquake forecasting. Earthquake prediction: An international review, 4, pp.43-51. DOI: 10.1029/ME004p0043

Morris, A., Ferrill, D.A., Henderson, D.B. (1996). Slip-tendency analysis and fault reactivation. Geology. 1996 Mar 1;24(3):275-8. DOI: 10.1130/0091-7613(1996)024<0275:STAAFR>2.3.CO;2

855   Muir Wood, R. and Mallard, D.J. (1992). When is a fault 'extinct'?. Journal of the Geological Society, 149(2), pp.251-254.
        https://doi.org/10.1144/gsjgs.149.2.0251

        National Emergency Management Agency (2012). Active fault map and seismic hazard map, Rep. NEMA-NATURE-2009-
        24, National Emergency Management Agency, 939 pp. (in Korean).

        NUMO (2004). Evaluating Site Suitability for a HLW Repository. Scientific Background and Practical Application of
860   NUMO's Siting Factors. Technical Report NUMO-TR-04-04, Nuclear Waste Management Organization of Japan (NUMO),
        August 2004. https://www.numo.or.jp/en/reports/pdf/Level3_SF_Final.pdf

        NUMO (2017). Japan -Nationwide_Map_of_Scientific_Features - Explanation material of the Nationwide Map of "Scientific
        Features" relevant for Geological Disposal. Ministry of Economy, Trade and Industry, Agency for Natural Resources and
        Energy. https://www.enecho.meti.go.jp/en/category/electricity_and_gas/nuclear/rwm/pdf/explanation_material.pdf

865   Ogata, S. and Honsho, S. (1981). Fault activity evaluation in the case of electric power plants. *Journal of the Japan Society of
        Engineering Geology*, *22*(1), pp.67-87. https://www.jstage.jst.go.jp/article/jjseg1960/22/1/22_1_67/_pdf/-char/ja

        Park, Y., Ree, J.H. and Yoo, S.H. (2006). Fault slip analysis of Quaternary faults in southeastern Korea. Gondwana Research,
        9(1-2), pp.118-125. DOI: 10.1016/j.gr.2005.06.007

        Park, Jong-Chan, Woohan Kim, Tae Woong Chung, Chang-Eob Baag and Jin-Han Ree (2007). Focal mechanisms of recent
870   earthquakes in the Southern Korean Peninsula. Geophys. J. Int. (2007) 169, 1103–1114. doi: 10.1111/j.1365-
        246X.2007.03321.x

        Park, Seung-Ik, Sung Won Kim, Sanghoon Kwon, Ngo Xuan Thanh, Keewook Yi, M. Santoshe (2013). Paleozoic tectonics
        of the southwestern Gyeonggi massif, South Korea: Insights from geochemistry, chromian-spinel chemistry and SHRIMP U–
        Pb geochronology, Gondwana Research (2013), http://dx.doi.org/10.1016/j.gr.2013.07.015

875   Park, S., Hong, T.K. and Rah, G. (2021). Seismic hazard assessment for the Korean Peninsula. Bulletin of the Seismological
        Society of America, 111(5), pp.2696-2719. https://doi.org/10.1785/0120200261

        POSIVA (2000). The site selection process for a spent fuel repository in Finland - Summary report. POSIVA 2000-15, by Tim
        McEwen,   EnvirosQuantiSci,   United   Kingdom;   Timo   Aikas   Posiva   Oy,   December   2000.
        https://inis.iaea.org/collection/NCLCollectionStore/_Public/32/030/32030717.pdf

880   Röckel, L., Ahlers, S., Müller, B., Reiter, K., Heidbach, O., Henk, A., Hergert, T., Schilling, F. (2022). The analysis of slip
        tendency of major tectonic faults in Germany. Solid Earth. 2022 Jun 29;13(6):1087-105.

        Rybicki, K., Kato, T. and Kasahara, K. (1985). Mechanical interaction between neighboring active faults: Static and dynamic
        stress field induced by faulting. *Bull. Earthquake Res. Inst. Univ. Tokyo*, *60*, pp.1-21.

        Schafmeister, M.T. (2023). High-level radioactive waste repository: How Geology combined with societal principles can lead
885   to public acceptance—the German experiment. Comptes Rendus. Géoscience, 355(S1), pp.1-15. DOI: 10.5802/crgeos.178

        SGD (2020). Fachliche Position der Staatlichen Geologischen Dienste Deutschlands (SGD) zu den Ausschlusskriterien des
        Standortauswahlgesetzes (StandAG) Ausschlusskriterium „Aktive Störungszonen" (§ 22 Abs. 2 Nr. 2 StandAG) 07.

Direktorenkreis der Staatlichen Geologischen Dienste Deutschlands, Baden-Württemberg 07. Oktober 2020. https://www.bgr.bund.de/Infogeo/DE/Downloads/2020_10_07_ausschlusskriterium_aktive_stoerungszonen.html

890   Sibson, R.H. (1985). A note on fault reactivation. Journal of Structural Geology, 7(6), pp.751-754. https://doi.org/10.1016/0191-8141(85)90150-6

SKB (2000). Technical Report TR-00-12: What requirements does the KBS-3 repository make on the host rock? Geoscientific suitability indicators and criteria for siting and site evaluation. Johan Andersson, Golder Grundteknik; Anders Ström, Christer Svemar, Svensk Kärnbränslehantering AB; Karl-Erik Almén, KEA Geo-Konsult AB; Lars O Ericsson, Chalmers University

895   of Technology, April 2000. https://www.skb.com/publication/17609

SKB (2004). Report R-04-17: Respect distances – Rationale and means of computation. Raymond Munier, Svensk Kärnbränslehantering AB, Harald Hökmark, Clay Technology, December 2004. https://www.skb.com/publication/670070

SKB, (2010). Technical Report TR-10-28: Design analysis report for the canister. Heikki Raiko, VTT; Rolf Sandström, Materials Science and Engineering, KTH Håkan Rydén, Magnus Johansson Svensk Kärnbränslehantering AB, April 2010.

900   https://www.osti.gov/etdeweb/servlets/purl/992698

SKB, (2011). SKB report R-11-07: Site selection – siting of the final repository for spent nuclear fuel, Svensk Kärnbränslehantering AB, March 2011. https://www.skb.com/publication/2204001/R-11-07.pdf

Soh, I., Chang, C., Lee, J., Hong, T.K., Park, E.S. (2018). Tectonic stress orientations and magnitudes, and friction of faults, deduced from earthquake focal mechanism inversions over the Korean Peninsula. Geophysical Journal International. 2018

905   May;213(2):1360-73. https://doi.org/10.1093/gji/ggy061

StandAG (2017). Gesetz zur Suche und Auswahl eines Standortes für ein Endlager für hochradioaktive Abfälle (Standortauswahlgesetz - StandAG). Issue date: 05.05.2017, full quote: "Site Selection Act of May 5, 2017 (BGBl. I p. 1074), which was last amended by Article 1 of the Act of December 7, 2020 (BGBl. I p. 2760)". https://www.gesetze-im-internet.de/standag_2017/BJNR107410017.html

910   Stein, Seth, Mian Liu, Eric Calais, Qingsong Li (2009). Mid-Continent Earthquakes as a Complex System. Seismological Research Letters Volume 80, Number 4 July/August 2009. doi: 10.1785/gssrl.80.4.551

Sun, C.G. and Kim, H.S. (2016). Geostatistical assessment for the regional zonation of seismic site effects in a coastal urban area using a GIS framework. *Bulletin of Earthquake Engineering*, *14*, pp.2161-2183. https://doi.org/10.1007/s10518-016-9908-5

915   Sun, C.G. and Kim, H.S. (2017). GIS-based regional assessment of seismic site effects considering the spatial uncertainty of site-specific geotechnical characteristics in coastal and inland urban areas. *Geomatics, Natural Hazards and Risk*, *8*(2), pp.1592-1621. DOI: 10.1080/19475705.2017.1364305

Torabi, A. and Berg, S.S. (2011). Scaling of fault attributes: A review. *Marine and petroleum geology*, *28*(8), pp.1444-1460. DOI: 10.1016/j.marpetgeo.2011.04.003

920   Torabi, A., Ellingsen, T.S.S., Johannessen, M.U., Alaei, B., Rotevatn, A. and Chiarella, D. (2020). Fault zone architecture and its scaling laws: where does the damage zone start and stop?. *Geological Society, London, Special Publications*, *496*(1), pp.99-124. https://doi.org/10.1144/SP496-2018-151

Tyagunov, S., Grünthal, G., Wahlström, R., Stempniewski, L. and Zschau, J. (2006). Seismic risk mapping for Germany. Natural Hazards and Earth System Sciences, 6(4), pp.573-586. www.nat-hazards-earth-syst-sci.net/6/573/2006/

925   Węglarczyk, S. (2018). Kernel density estimation and its application. In ITM web of conferences (Vol. 23, p. 00037). EDP Sciences. https://doi.org/10.1051/itmconf/20182300037

Wells, Donald L., and Kevin J. Coppersmith (1994). New Empirical Relationships among Magnitude, Rupture Length, Rupture Width, Rupture Area, and Surface Displacement. Bulletin of the Seismological Society of America, Vol. 84, No. 4, pp. 974-1002, August 1994. DOI: 10.1785/BSSA0840040974

930   Xie, Linmao, Min Ki-Bok (2016). Initiation and propagation of fracture shearing during hydraulic stimulation in enhanced geothermal system. Geothermics. 2016 Jan 1;59:107-20. DOI: 10.1016/j.geothermics.2015.10.012

Yuan, Kunxiaojia; Cheng, Xiaoqiang; Gui, Zhipeng; Li, Fa; Wu, Huayi (2019). A quad-tree-based fast and adaptive Kernel Density Estimation algorithm for heat-map generation. International Journal of Geographical Information Science, Volume 33, 2019 - Issue 12, 1–22. doi:10.1080/13658816.2018.1555831

935   Yun, H.W., Kim, J.R., Yoon, H., Choi, Y. and Yu, J. (2019). Seismic Surface Deformation Risks in Industrial Hubs: A Case Study from Ulsan, Korea, Using DInSAR Time Series Analysis. Remote Sensing, 11(10), p.1199. https://www.mdpi.com/2072-4292/11/10/1199